# A new probe for super-resolution imaging of membranes elucidates trafficking pathways

Natalia H. Revelo,[1,2,5,6] Dirk Kamin,[1,2] Sven Truckenbrodt,[1,2,8] Aaron B. Wong,[3,5,6] Kirsten Reuter-Jessen,[4,6] Ellen Reisinger,[4,6] Tobias Moser,[3,6,7] and Silvio O. Rizzoli[1,2,6,7]

[1]Department of Neuro- and Sensory Physiology; [2]European Neuroscience Institute; and [3]InnerEarLab and [4]Molecular Biology of Cochlear Neurotransmission Group, Department of Otolaryngology; University Medical Center Göttingen, 37099 Göttingen, Germany
[5]International Max Planck Research School for Neurosciences, 37077 Göttingen, Germany
[6]Collaborative Research Center 889 and [7]Cluster of Excellence Nanoscale Microscopy and Molecular Physiology of the Brain, University of Göttingen, 37099 Göttingen, Germany
[8]International Max Planck Research School for Molecular Biology, 37077 Göttingen, Germany

The molecular composition of the organelles involved in membrane recycling is difficult to establish as a result of the absence of suitable labeling tools. We introduce in this paper a novel probe, named membrane-binding fluorophore-cysteine-lysine-palmitoyl group (mCLING), which labels the plasma membrane and is taken up during endocytosis. It remains attached to membranes after fixation and permeabilization and can therefore be used in combination with immunostaining and super-resolution microscopy. We applied mCLING to mammalian-cultured cells, yeast, bacteria, primary cultured neurons, *Drosophila melanogaster* larval neuromuscular junctions, and mammalian tissue. mCLING enabled us to study the molecular composition of different trafficking organelles. We used it to address several questions related to synaptic vesicle recycling in the auditory inner hair cells from the organ of Corti and to investigate molecular differences between synaptic vesicles that recycle actively or spontaneously in cultured neurons. We conclude that mCLING enables the investigation of trafficking membranes in a broad range of preparations.

## Introduction

Eukaryotic cells rely on membrane recycling for a variety of pathways, such as secretion of solutes, nutrient uptake, or membrane protein turnover. Each pathway uses several types of organelles, from the plasma membrane, the ER, and the Golgi apparatus to recycling intermediates, such as carrier or transport vesicles (Bonifacino and Glick, 2004). Establishing the identities of the different organelles and recycling intermediates that function in a given pathway is a complex task. Both the recycling membranes and the protein markers of the different organelles need to be identified simultaneously.

This task could be performed by labeling the membrane of the recycling organelle with a fluorophore and using immunostaining procedures to reveal the protein markers on the same organelle. This has been surprisingly difficult to achieve, although endocytosis and exocytosis have been visualized by fluorescent probes, such as styryl (FM) dyes, for more than two decades (Betz et al., 1992). The main problem has been that the membrane probes commonly used for live-cell imaging are only poorly fixed during immunostaining procedures. This is the case even for the fluorophores that contain one lysine residue, such as the fixable FM dyes or fixable dextran particles. The probes are therefore lost from their target organelles and may even become trapped in other structures such as mitochondria. A second problem derives from the fact that a multitude of trafficking organelles are in close proximity to each other, making it difficult for conventional diffraction-limited microscopy to discriminate them. Therefore, super-resolution microscopy is needed (Hell, 2007), albeit most available membrane probes have not been optimized for use in super-resolution microscopy.

N.H. Revelo and D. Kamin contributed equally to this paper.

Correspondence to Silvio O. Rizzoli: srizzol@gwdg.de; or Dirk Kamin: dirk.kamin@mpibpc.mpg.de

D. Kamin's present address is Dept. of NanoBiophotonics, Max Planck Institute for Biophysical Chemistry, 37077 Göttingen, Germany.

Abbreviations used in this paper: BPB, bromophenol blue; IHC, inner hair cell; LDL, low-density lipoprotein; mCLING, membrane-binding fluorophore-cysteine-lysine-palmitoyl group; PLL, poly-L-lysine; ROI, region of interest; STED, stimulated emission depletion.



The Rockefeller University Press $30.00
J. Cell Biol. Vol. 205 No. 4 591–606
www.jcb.org/cgi/doi/10.1083/jcb.201402066

To overcome these limitations, we developed a novel membrane probe, named membrane-binding fluorophore-cysteine-lysine-palmitoyl group (mCLING), composed of a short polypeptide coupled to a membrane anchor and to a fluorophore (Fig. 1, A and B). The latter can be freely chosen by the investigator, according to the type of microscopy required. mCLING was taken up during membrane trafficking, was efficiently fixed during immunostaining, and allowed the identification of different organelles and membrane-recycling intermediates. We demonstrate here the value of this new probe in several systems, from conventional cell cultures to a demanding tissue preparation, the organ of Corti of the mammalian ear.

## Results

### A novel membrane probe for investigating endocytosis

We set out to develop a membrane probe that does not come off membranes during recycling, that is optimally fixable, and that can be used in immunostaining (Fig. 1 A). Commercially available membrane probes were not suitable for such experiments. They typically consist of fluorophores coupled to lipid chains, which are not optimally fixable (Fig. 1, E–J). An additional path we explored was the use of fluorescently coupled polypeptide chains, which should be more easily fixed. However, they were also removed from membranes upon fixation and permeabilization (Fig. S1, A and B).

We reasoned that small polypeptide chains could be induced to remain on membranes during fixation by coupling them to a lipid tail. Based on this idea, we developed a probe consisting of an octapeptide with one cysteine and seven lysines, one of which was bound to a palmitoyl tail (Fig. 1 B). A maleimide group bridged the cysteine to the fluorophore (in our case, Atto647N, obtained from ATTO-TEC; any dye compatible with maleimide coupling could, in principle, be used). We termed this probe mCLING. It has a molecular weight of 2,056 D, including the Atto647N moiety.

mCLING labeled the plasma membranes of cultured cells and was taken up by endocytosis (Fig. 1, C and D). The labeling pattern of mCLING was identical to that of FM dyes in living cells (Fig. 1 E), confirming that this probe indeed reports endocytosis. mCLING did not have toxic effects on the cells (Fig. S1, C–G).

The advantage of mCLING over FM dyes became evident upon fixation. FM dyes were largely lost from the membranes and had a tendency to end up in organelles resembling mitochondria (Fig. 1, F–I). This was the case not only for FM 1-43 (Fig. 1 G) but also for fixable FM variants, which contain one amine moiety (Fig. 1, H [AM 1-43] and I [FM 4-64FX]). This suggests that one amine moiety is insufficient for optimal fixation. In contrast, mCLING remained on the membranes after fixation and did not label mitochondria (Fig. 1 F).

A quantitative assessment of probe fluorescence in living, fixed, or permeabilized cells confirmed that mCLING is optimally retained by the membranes (Fig. 1 J). This is also in line with its slow wash-off kinetics (Fig. 1 K). In contrast, most of the FM 1-43 fluorescence is lost from the membranes upon fixation, and it is difficult to detect after permeabilization (Fig. 1 J). Fixable FM dyes (AM 1-43 or FM 4-64FX) are retained better within the cells upon fixation (Fig. 1 J), although, as mentioned in the first paragraph of the Results, they now label mitochondria, rather than endocytotic membranes (Fig. 1, H and I). Finally, both fixable FM dyes are lost upon permeabilization (Fig. 1 J).

### mCLING can be used to reveal endocytotic organelles in mammalian cultured cells

We next sought to verify whether mCLING can label different types of endocytotic organelles, including those involved in the traffic of cellular ligands such as transferrin, low-density lipoprotein (LDL), and EGF. We applied these ligands to COS7 cells in culture, in the presence of mCLING. Live epifluorescence imaging showed that virtually all ligand-containing organelles were also labeled by mCLING (Fig. 2 A). This was also the case when the cells were investigated by confocal microscopy after fixation (Fig. 2 B). Finally, mCLING remained attached to the membranes of these organelles after permeabilization, which enabled us to immunostain the organelles (Fig. 2 C).

Importantly, the presence of mCLING did not interfere with membrane trafficking in COS7 cells. For example, the amount of transferrin uptake was not affected by mCLING; its recycling and release were also unaffected (Fig. S1 F).

### mCLING, but not FM 4-64, can be used in conjunction with immunostaining in yeast

The red-shifted styryl dye FM 4-64 has been used for almost two decades in *Saccharomyces cerevisiae* yeast (Vida and Emr, 1995). It reveals endocytotic organelles in living yeast cells (Fig. 3 A). However, it is lost during fixation, and it provides a diffuse, poor labeling after permeabilization and immunostaining (Fig. 3 A).

mCLING revealed the plasma membrane and endocytotic organelles in living yeast, in a pattern indistinguishable from that of FM 4-64. Unlike this dye, however, mCLING was retained during fixation and also remained in the organelles after permeabilization and immunostaining (Fig. 3, B–D). This suggests that mCLING is compatible with yeast imaging.

### mCLING, but not FM 1-43, can be used in super-resolution microscopy of bacteria

We compared FM dyes with mCLING in bacterial membranes. We applied FM 1-43, which is the brightest styryl dye, or mCLING to *Escherichia coli* bacteria for a few minutes. We then imaged the cells in LB (lysogeny broth) medium, without fixation.

Both FM 1-43 and mCLING revealed the membranes of the bacteria (Fig. S2, A and B). However, FM dyes are not compatible with super-resolution microscopy and, therefore, only provided a blurry pattern of the bacterial membrane. In contrast, the Atto647N dye coupled to mCLING is ideal for stimulated emission depletion (STED) microscopy. In this technique, the focal volume is modulated to obtain a resolution ∼16-fold higher than that of confocal microscopy in the x–y plane (Hoopmann et al., 2010). The higher resolution provided much more precise images of *E. coli* membranes (Fig. S2 B). This will enable investigators to study the precise distribution of various molecules on the *E. coli* membrane in the future.

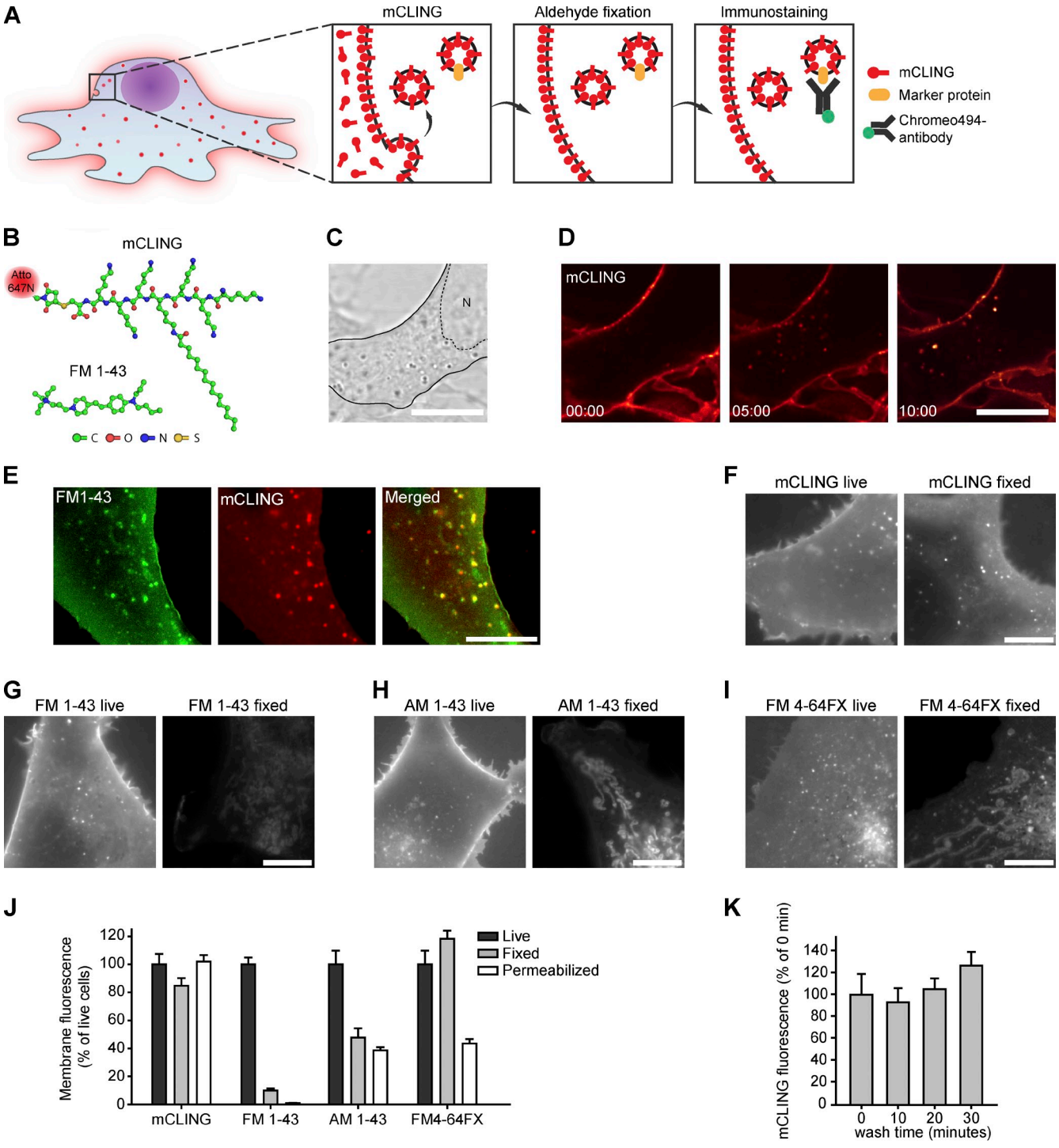


Figure 1. **mCLING: A novel membrane probe.** (A) Outline of an experiment designed to reveal the molecular composition of endocytotic organelles. The membrane probe mCLING labels the endocytotic organelles and is retained during fixation and immunostaining. Different protein markers can thus be analyzed on the endocytotic organelles. (B) The structure of mCLING compared with the smaller styryl dye FM 1-43. (C) Outline of a cultured cell (COS7) in bright-field microscopy. N marks the nucleus (dashed outline). (D) Uptake of mCLING in endocytotic organelles, visualized by confocal microscopy. (E) Live epifluorescence imaging of COS7 cells, co-incubated for 5 min with FM 1-43 and mCLING. Note the high colocalization of the two probes. (F–I) Comparison between live and fixed COS7 cells, incubated with mCLING (F), FM 1-43 (G), AM 1-43 (H), and FM 4-64FX (I). (J) Quantification of the fluorescence intensity of these four membrane probes in living, fixed, or fixed and permeabilized cells (21–37 cells evaluated in every condition). (K) Quantification of mCLING wash-off kinetics. COS7 cells were incubated with mCLING for 5 min and then washed for different time periods (24–28 cells evaluated for every incubation time point). Error bars show SEMs. Bars, 10 µm.

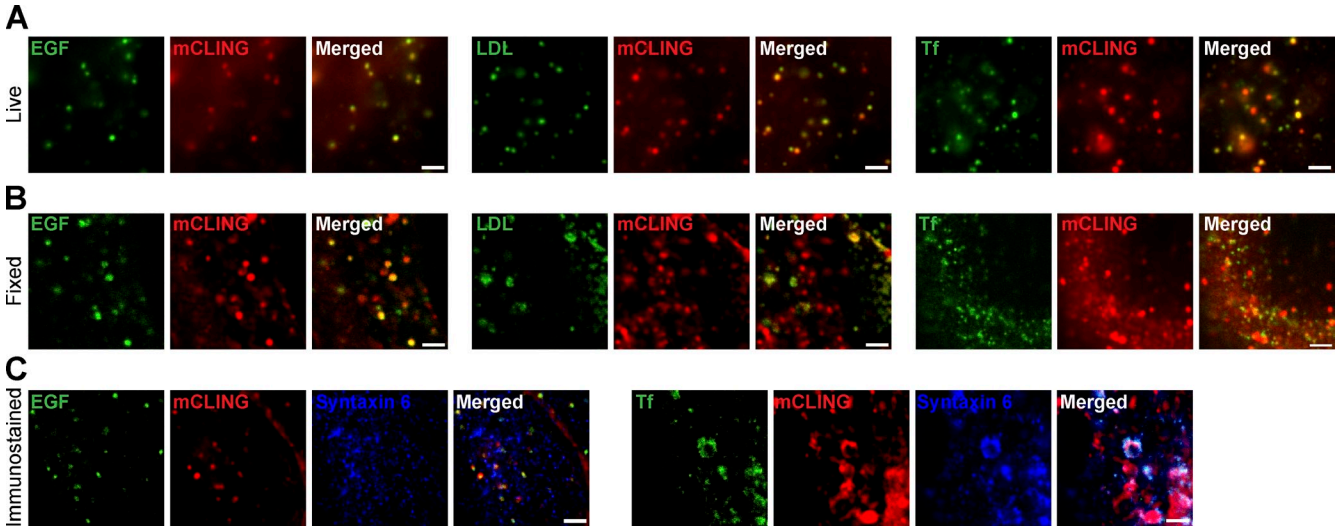


Figure 2. **mCLING labels endocytotic organelles involved in ligand trafficking.** (A) COS7 cells were incubated for 5 min with mCLING and with fluorescently coupled transferrin (Tf), LDL, or EGF at 37°C. The living cells were then analyzed by epifluorescence imaging. (B) The correlation of mCLING with the ligands is also evident after fixation, in confocal microscopy. (C) We immunostained cells after incubation with mCLING and transferrin or EGF. LDL was not used because it does not fix well and is lost during permeabilization. Note that mCLING still correlates with the ligand-labeled organelles. Immunostaining reveals that these organelles contain the endosomal SNARE protein syntaxin 6. Bars, 2 µm.

### Super-resolution imaging of mCLING reports endocytosis in inner hair cells (IHCs)

We originally developed mCLING to study synaptic vesicle recycling pathways in the auditory IHCs from the organ of Corti of mice because the use of endocytotic markers, and especially FM dyes, has been highly controversial in this preparation. The IHCs are presynaptic cells that do not have synaptic boutons. They release neurotransmitter by exocytosis at active zones, which are located in the basal region of the cell and which are characterized by synaptic ribbons, specialized proteinaceous structures that tether synaptic vesicles and promote their release (Glowatzki and Fuchs, 2002; Goutman and Glowatzki, 2007; Matthews and Fuchs, 2010; Pangršič et al., 2012). After exocytosis, the vesicles are recycled from the plasma membrane, through mechanisms that are still unclear. A main difficulty in IHCs has been that FM dyes have been shown to penetrate through the mechanotransducer channels into their cytosol, labeling the IHCs nonspecifically (Gale et al., 2001; Meyers et al., 2003; Kamin et al., 2014). Therefore, a larger probe with the properties of mCLING would be desirable.

We studied the uptake of mCLING in the organ of Corti (dissected from 14- to 18-d-old wild-type mice and used within 5–10 min after dissection), focusing on the IHCs (Fig. 4 A). Unlike FM 1-43, mCLING did not rapidly and diffusely stain the IHC

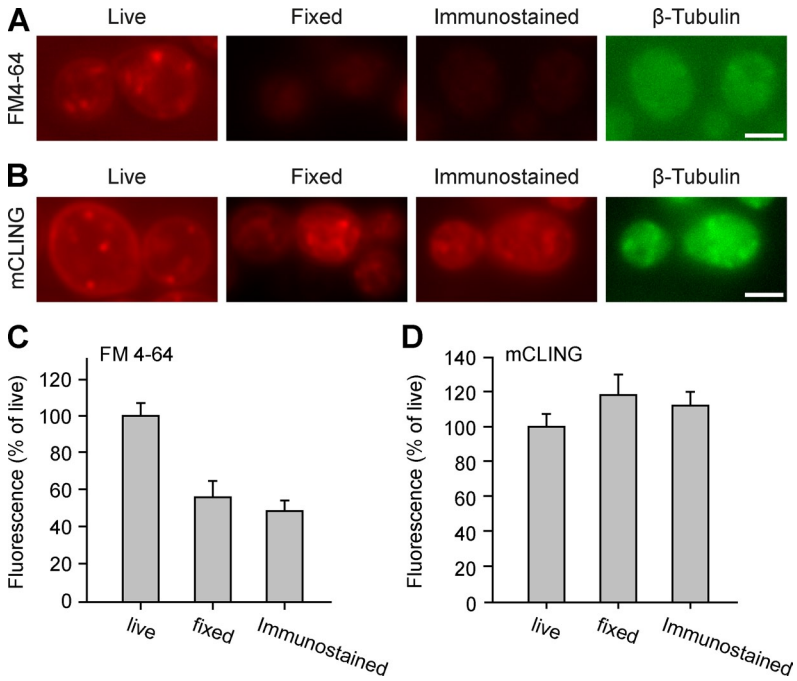


Figure 3. **mCLING imaging in yeast.** (A) Yeast cells from the strain BY4742 were incubated with FM 4-64 for 20 min, at RT, and were analyzed by epifluorescence imaging under different conditions: live (left), after fixation for 30 min with 4% PFA + 0.2% glutaraldehyde (middle), or after permeabilization and immunostaining for tubulin, using an antitubulin single-chain recombinant antibody (right; Nizak et al., 2003). (B) The cells were treated similarly, using mCLING. (C and D) Quantification of the FM4-64 or mCLING fluorescence levels. 17–31 fields of yeast cells were analyzed for each condition. Error bars show SEMs. Bars, 2 µm.

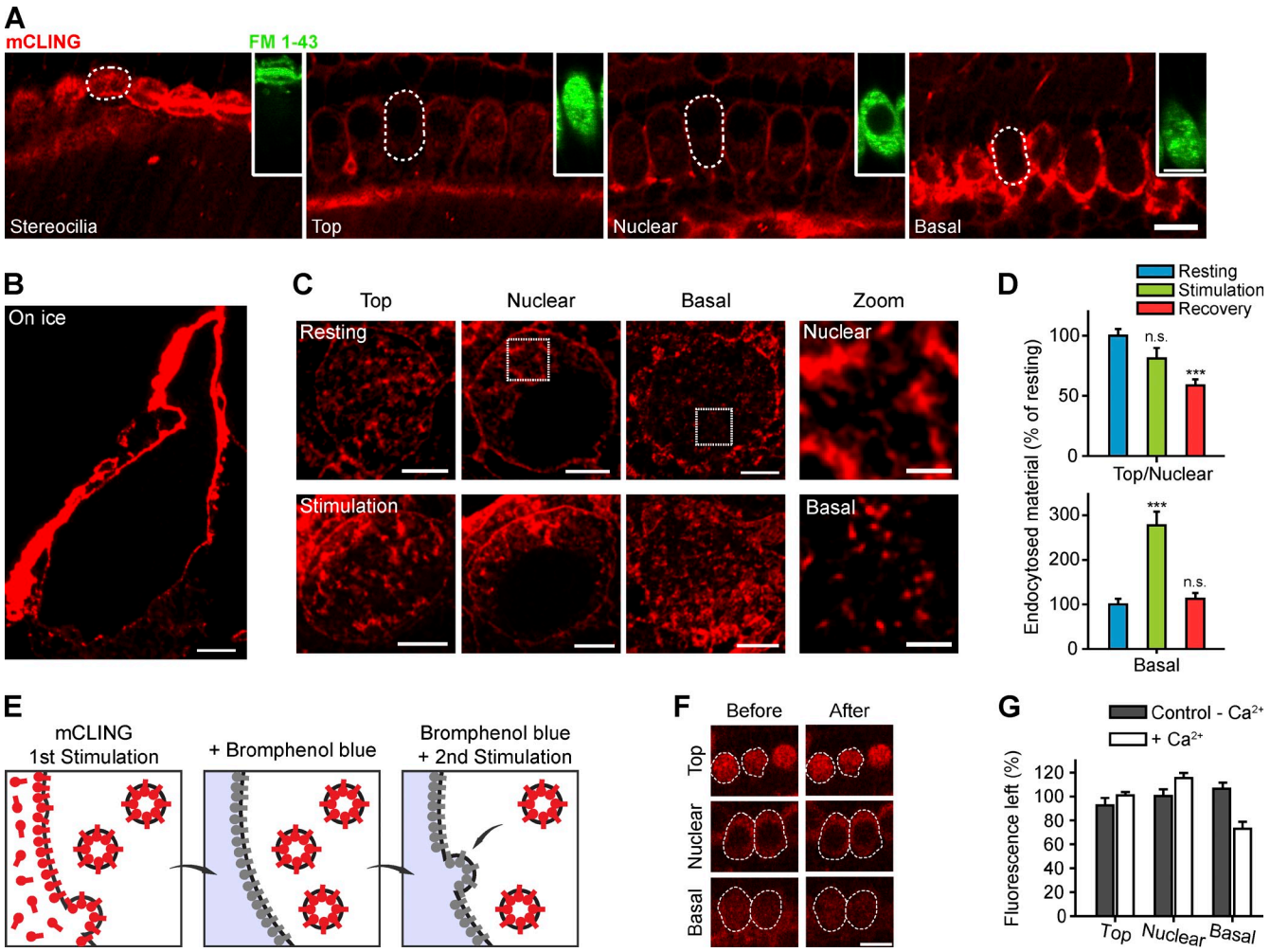


Figure 4. **mCLING imaging in IHCs.** (A) mCLING does not permeate mechanotransducer channels in living IHCs. Confocal images of the stereocilia bundle and of the top, nuclear, and basal levels of a row of living IHCs were taken after a 3-min incubation with 1.7 µM mCLING. mCLING is found inside the cells, presumably taken up by endocytotic organelles, but does not diffusely label the cells as seen for FM 1-43 (green insets), which enters the cytosol through the mechanotransducer channels. The dashed lines show the profile of one IHC at the different imaged planes. (B) STED microscopy image of a plastic section from an IHC incubated with mCLING at low temperature. Endocytosis is inhibited. (C) When incubated at 37°C, mCLING was found in structures of different sizes, both in resting cells (top) and in stimulated cells (bottom). The zoom images indicate typical organelles from the top/nuclear and basal regions of IHCs (boxes). (D) Stimulation increases mCLING labeling only in the basal region of the cells. The error bars show means ± SEM from 27, 22, and 57 cell top and nuclear regions (resting, stimulation, and recovery, respectively) and from 25, 28, and 27 cell bases (resting, stimulation, and recovery, respectively). n.s., no significant difference (*t* test, $P > 0.05$); ***, significant difference (*t* test, $P \leq 0.001$) compared with resting condition. (E) Experimental outline for the investigation of exocytosis using mCLING: cells are stimulated in the presence of mCLING (65 mM KCl for 1 min), which is taken up in organelles. After a brief wash, BPB is added to quench the dye present on the cell surface (for 5 min). A second round of stimulation in the presence of BPB (65 mM KCl for 1 min) causes the exocytosis of labeled organelles, whose fluorescence is quenched. (F) Typical fluorescence images of top, nuclear, and basal regions of IHCs (dashed lines) treated with BPB, before (left) or after the second round of stimulation (right). (G) Quantification of the fluorescence intensity remaining after the second round of stimulation (white bars). As a control, we analyzed cells stimulated in the absence of $Ca^{2+}$ during the second round (gray bars). All measurements are normalized to their initial intensity values, before stimulation. A significant decrease is only obtained for the basal region of the cells (*t* test, $P < 0.001$; two to six independent experiments were performed, with 8–15 IHCs analyzed in each experiment). Error bars show SEMs. Bars: (A and F) 10 µm; (B and C, main images) 2 µm; (C, zoom images) 500 nm.

apex (where the mechanotransducer channels are located), indicating that it does not enter through channels into the cells (Fig. 4 A).

We then investigated the IHCs using STED microscopy. As the axial resolution of STED is comparable to that of conventional microscopy (500–600 nm), we increased our imaging precision by embedding the mCLING-stained samples in a plastic resin (melamine; TCI Europe) and by processing them into thin (100–200 nm) sections. The resulting images thus have a resolution of at least ~50–60 nm in the x–y plane and 100–200 nm along the z axis. At this resolution, the plasma membrane staining tends to appear nonuniform, especially in immunostained preparations. This is probably caused by the holes induced in the membrane by the fixation procedure and the detergent permeabilization. This phenomenon is evident in all permeabilized membranes, including those of hippocampal cultured neurons (see Figs. 8–10).

mCLING only labeled the extracellular membrane of IHCs at low temperatures, but it was taken up into endocytotic organelles at physiological temperature (Fig. 4, B and C). Endocytotic organelles formed throughout the IHC, both at rest and during stimulation by depolarization with KCl (Fig. 4 C), indicating that constitutive membrane traffic is relatively strong in IHCs. Tubular organelles were abundant in the nuclear and top (supranuclear)

regions, whereas the basal region mainly contained numerous smaller, vesicle-like objects (Fig. 4 C).

mCLING uptake was substantially reduced by inhibitors for two proteins involved in endocytosis, clathrin and dynamin (Fig. S3, A and B). Moreover, the amount of internalized mCLING signal was also strongly inhibited in a mouse line that lacks otoferlin, as shown in Fig. S3 (C and D, *Otof*$^{-/-}$ mice; Reisinger et al., 2011). Otoferlin is involved in synaptic vesicle exocytosis (Roux et al., 2006; Pangršič et al., 2010) and possibly also in the coupling of exo- and endocytosis (Duncker et al., 2013). Overall, these experiments demonstrate that mCLING indeed reports endocytotic membrane uptake in IHCs.

### mCLING can reveal not only endocytosis, but also exocytosis, thereby demonstrating that synaptic vesicles recycle in the basal region of the IHCs

As indicated in Fig. 4 C, mCLING uptake was observed both at rest and during IHC depolarization (stimulation) throughout the cell. To determine which of the organelles were relevant to synaptic vesicle recycling, we analyzed the changes in the amount of IHC uptake during stimulation. We found that the basal region, where the active zones are located, responded strongly to stimulation, with a more than twofold increase in endocytosis, whereas no such increase was observed elsewhere (Fig. 4 D).

We sought to verify this finding by imaging the exocytosis of mCLING-labeled organelles in living cells. This experiment is often performed with FM dyes (Betz et al., 1992), monitoring the release and wash off of the dyes from exocytosing vesicles. Because mCLING binds to membranes far more strongly than FM dyes and therefore cannot be washed off during exocytosis (Fig. 1 K), we quenched the fluorescence of the Atto647N dye of mCLING on the cell surface to achieve the same effect. For this, the cells were labeled with mCLING during one stimulation round (as in Fig. 4 C) and then stimulated again in presence of bromophenol blue (BPB; Fig. 4 E). BPB quenches Atto647N fluorescence (as already noted in the past for both FM dyes and fluorescent proteins; see for example Harata et al., 2006). Fluorescence was detected in presence of BPB in all areas of the cell—top, nuclear, or basal (Fig. 4 F). After stimulation in presence of BPB, the fluorescence appeared unchanged in the top and nuclear areas, although it was lower in the bottom area (Fig. 4 F, right). A quantification of the fluorescence intensities verified this observation (Fig. 4 G, white bars). Stimulation of IHCs in presence of BPB, but in the absence of $Ca^{2+}$ (to inhibit exocytosis), resulted in no changes in fluorescence (Fig. 4 G, gray bars). This confirms that the drop in mCLING fluorescence in the basal region of the IHCs is related to synaptic vesicle exocytosis. Finally, we also verified this conclusion by an independent technique, pHluorin imaging (Fig. S3, E–H; Miesenböck et al., 1998).

### mCLING reveals the morphology of the organelles that recycle synaptic vesicles in the basal region of IHCs

Electron microscopy and electron tomography studies of ribbon synapses have suggested in the past that membrane is taken up near the release sites in the form of membrane infoldings and cisterns (round organelles larger than synaptic vesicles, not attached to the plasma membrane) as well as coated vesicles (for example, Siegel and Brownell, 1986; Lenzi et al., 2002; Frank et al., 2010).

This type of investigation has been so far achievable only with electron microscopy. We sought to test whether mCLING can provide comparable data in fluorescence microscopy. We studied the morphology of mCLING-labeled organelles in the basal region of IHCs. We immunostained the cells for Ribeye, a major component of the synaptic ribbon located next to the IHC active zone (Schmitz et al., 2000; Khimich et al., 2005). Stimulation resulted in the appearance of mCLING fluorescence in the vicinity of the ribbons, both when using strong depolarizations (65 mM KCl for 1 min) or mild ones (10 or 25 mM KCl for 1 min; Fig. 5 A). A large proportion of the mCLING-labeled organelles was clearly separated from the plasma membrane, similar to the cisterns observed in electron microscopy after stimulation of hair cells (Lenzi et al., 2002). However, others appeared continuous with the membrane bordering the IHCs and, therefore, may have been similar to the membrane infoldings described in electron microscopy experiments of stimulated IHCs (41 ± 4.2%, $n = 4$ independent experiments in 65 mM KCl stimulation; Fig. 5 A. See also Neef et al., 2014).

As would be expected for synaptic vesicle recycling intermediates, neither the infoldings nor the cisterns persisted long after the end of stimulation. They disappeared from the active zone areas within a few minutes, being replaced with small organelles that were compatible with the size of synaptic vesicles (Fig. 5, A [bottom row] and B). Labeling more vesicles by a second round of stimulation also allowed us to observe labeled vesicles that remained in the active zone areas (Fig. 5 C). Finally, electron microscopy experiments confirmed the presence of both cisterns and infoldings as well as their eventual breakup into small vesicles (Kamin et al., 2014).

### mCLING labeling can be coupled with immunostaining to reveal the nature of the different endocytotic organelles in IHCs

A major difficulty in interpreting endocytosis and membrane trafficking in IHCs has been that synaptic vesicle recycling shares the cell body of the IHC with many other organelles involved in constitutive membrane trafficking. These include the endosomes of the secretory and receptor-recycling pathways and the different carrier vesicles of the membrane-to-Golgi or ER-to-Golgi pathways. These pathways take place at the same time, which makes it difficult to separate the organelles from the different pathways. It is therefore not surprising that many organelles have been implicated in the past in synaptic vesicle recycling in IHCs or similar cells: (a) the ER (Griesinger et al., 2004); (b) the Golgi apparatus (see Siegel and Brownell, 1986; Griesinger et al., 2005); (c) tubular organelles in different regions of the cell (Spicer et al., 1999, 2007); (d) membrane infoldings and cisterns (Siegel and Brownell, 1986; Lenzi et al., 2002; Frank et al., 2010); and (e) endosome-like organelles in the apical region of IHCs, in the vicinity of the cuticular plate that tops the cells (Griesinger et al., 2002, 2004; see also Kachar et al., 1997). It is probable that some of these

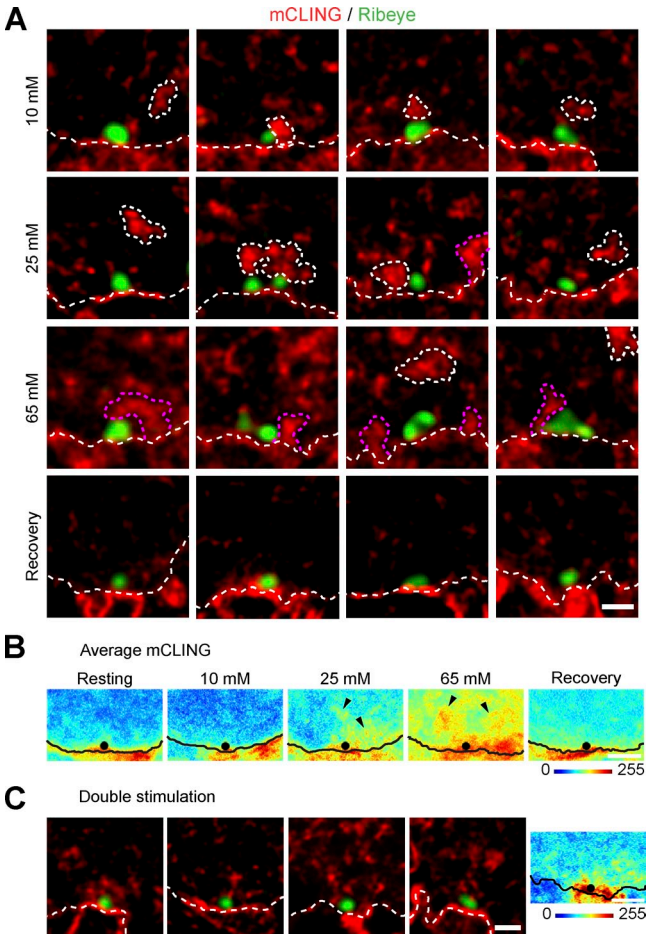


Figure 5. **mCLING reveals organelles endocytosed at the IHC base.** (A) Endocytosis near active zones, at the base of the cell, during stimulation. mCLING-labeled organelles were imaged in the vicinity of synaptic ribbons (green). Several mCLING-labeled membrane infoldings and internalized organelles are indicated by the dashed white lines. Similar lines indicate the plasma membrane. Organelles that appear connected to the plasma membrane are indicated by the dashed pink lines. The different images show organelles appearing after stimulation (depolarization for 1 min with 10, 25, or 65 mM KCl) and after recovery from 65 mM KCl depolarization (5 min in $Ca^{2+}$-containing buffer). (B) To obtain a more quantitative view of endocytosis across different release sites, average images centered on the synaptic ribbons were generated (from 20 to 31 individual ribbon synapses). The black lines show the estimated location of the plasma membrane in the average images, and the black dots indicate the location of the ribbons. Note the increase on average mCLING fluorescence intensity in stimulated active zones (black arrowheads). (C) A similar analysis of IHCs that were subjected to two rounds of stimulation (65 mM KCl for 1 min each). The double-stimulated cells contained more labeled organelles in the basal region of the cells than the cells stimulated only once, as expected (compare with bottom row of cells in A). (right) Several of these organelles find themselves close to the synaptic ribbon, as indicated also by the average image. White dashed lines indicate the plasma membrane. Bars: (A and C, left) 500 nm; (B and C, right) 1 µm.

organelles are involved in constitutive traffic and not in synaptic vesicle recycling.

It has not been possible so far to distinguish between these possibilities, as the molecular identities of the different endocytotic organelles could not be determined. We have therefore combined mCLING with immunostaining for different organelle markers, in two-color STED microscopy (Fig. 6).

First, we found that synaptic vesicle markers, such as the VGLUT3 (vesicular glutamate transporter 3) and Rab3 (Ruel et al., 2008; Seal et al., 2008), colocalized with endocytotic organelles only at the base of IHCs (Fig. 6, A and B). This demonstrates that synaptic vesicle recycling does indeed take place at the basal pole of these cells.

Second, otoferlin, an IHC protein that is currently the subject of intense investigation (Pangršič et al., 2012; Duncker et al., 2013) and which appears to be involved in both exocytosis and endocytosis, correlated with most of the newly endocytosed organelles, throughout the IHCs (Fig. 6, C and H). This suggests that otoferlin is involved in clathrin-mediated endocytosis in general and not only in synaptic vesicle endocytosis (see further discussion in Duncker et al., 2013).

Third, none of the organelles we investigated colocalized with ER or Golgi markers (Fig. 6, D and E), neither the vesicles from the basal region of the IHCs nor the tubular structures from the nuclear and top regions. The latter did contain SNARE molecules that are typically found on recycling endosomes (syntaxin 6 and syntaxin 16; Fig. 6, F and G). The tubular organelles are thus probably similar to the recycling endosomes from fibroblast cells, which are involved in the traffic between the plasma membrane and the trans-Golgi apparatus (Mallard et al., 2002; Brandhorst et al., 2006; Jahn and Scheller, 2006). Vti1a (Vps10p-tail-interactor-1a), a SNARE molecule that is found typically on early endosomes and less on recycling endosomes, colocalized more poorly with the mCLING-labeled organelles (Fig. 6 H), confirming the hypothesis that these are similar to recycling endosomes. Fourth, the apical endocytotic organelles (Kachar et al., 1997) were also of endosomal nature because a sizeable fraction of these organelles correlated with the late endosome/lysosome marker LAMP1 (lysosome membrane–associated protein 1; Fig. S4).

## A simple and inexpensive approach to perform multicolor super-resolution imaging using mCLING and immunostaining

The imaging approach we used so far (two-color STED microscopy) did not allow us to correlate two organelle markers with mCLING at the same time. Because two-color STED microscopy is also an expensive approach, requiring a specialized microscopy setup, we sought to use mCLING in a simpler and cheaper fashion.

We therefore developed an approach in which we could use mCLING in multicolor imaging on conventional epifluorescence setups, relying on increasing z-axis discrimination. We immunostained organs of Corti labeled with mCLING under stimulation (65 mM for 1 min), for VGLUT3 and otoferlin, for VGLUT3 and syntaxin 6, for otoferlin and syntaxin 16, and finally, for syntaxin 6 and syntaxin 16. We cut the samples into ∼20-nm sections and imaged them by epifluorescence microscopy. The high z resolution (25- to 30-fold higher than confocal imaging) allowed us to measure the signal from only a few primary antibodies in each labeled organelle and thus enabled us to investigate the correlation between the different protein markers in the different cell regions (Fig. 7 A). The results we obtained (Fig. 7 B) confirmed the suggestions made from STED

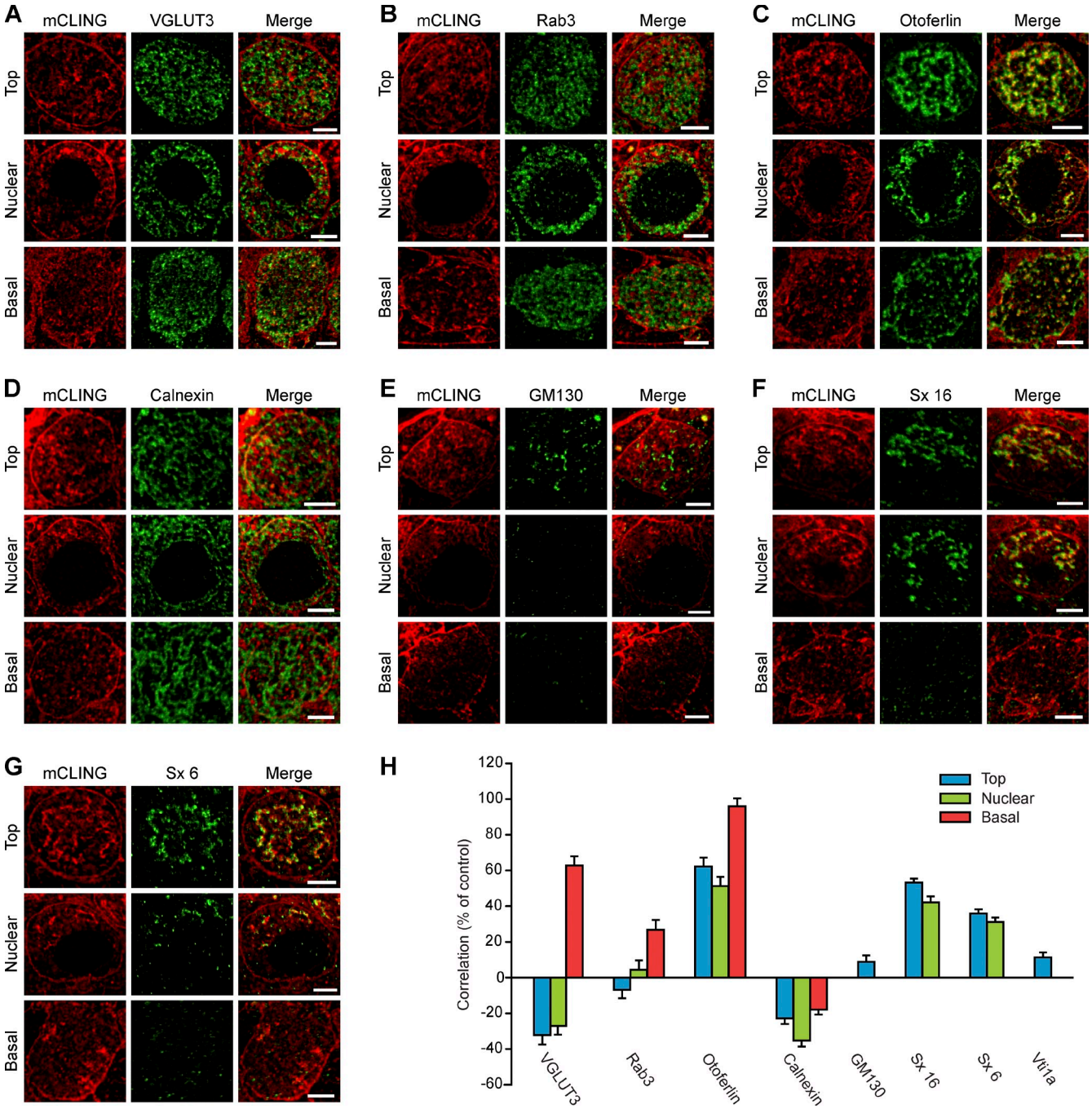


Figure 6. **Immunostaining analysis of the organelles involved in membrane recycling in IHCs.** We labeled organs of Corti with mCLING and then immunostained them for different organelle markers. (A–G) The following markers were analyzed using two-color STED: VGLUT3, a synaptic vesicle marker (A); Rab3, a second synaptic vesicle marker (B); the synaptic protein otoferlin (C); the ER marker calnexin (D); the cis-Golgi apparatus marker GM130 (E); and the SNARE proteins syntaxin 16 (Sx 16) and syntaxin 6 (Sx 6), markers for endosomes (F and G). (H) Pearson's correlation coefficients were determined for each immunostaining condition. For the markers present throughout the cell, the correlation coefficients were calculated at all the different levels of the cell (top, nuclear, and basal). For markers abundant only at the top (or the top/nuclear) level, the analysis was not performed at other levels. The correlation with an additional endosomal marker, the SNARE Vti1a, is also shown. Coefficients are expressed as percentages of the maximum expected correlation (% of control) obtained from two-color immunostaining of VGLUT3 using Atto647N- and Chromeo494-coupled secondary antibodies. Error bars represent mean correlation coefficient ± SEM (from 100 to 500 mCLING-labeled organelles, from 20 to 85 cells, in two to six independent experiments for each marker protein). Bars, 2 µm.

microscopy (Fig. 6). These observations allowed us to generate a model of membrane trafficking in IHCs (Fig. 7 C), which separates for the first time the endocytotic organelles that function in constitutive pathways from those involved in synaptic vesicle recycling.

### mCLING can be applied to the *Drosophila melanogaster* larva neuromuscular junction

We next sought to test mCLING in conventional synapses, from a different tissue preparation. We first turned to a large synaptic bouton, from the *Drosophila* larva neuromuscular junction (see

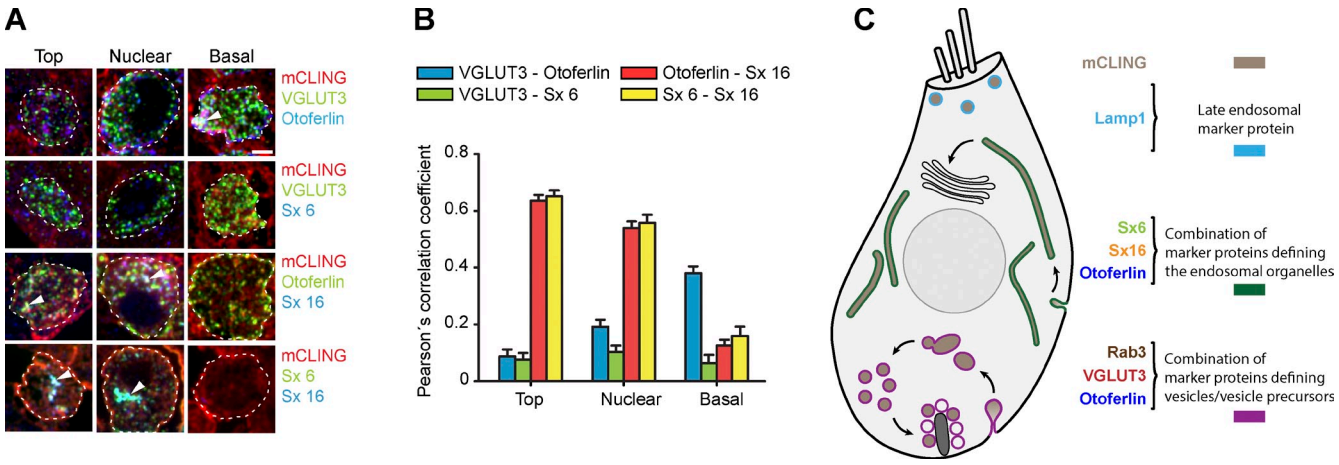


Figure 7. **Multicolor immunostaining analysis of the IHC organelles.** (A) mCLING-labeled organs of Corti were immunostained for VGLUT3 and otoferlin (first row), for VGLUT3 and syntaxin 6 (Sx 6; second row), for otoferlin and syntaxin 16 (Sx 16; third row), and finally for syntaxin 6 and syntaxin 16 (fourth row). The samples were cut into 20-nm sections and were imaged using an epifluorescence microscope. Dashed white lines indicate the plasma membrane of the IHCs. White arrowheads point to organelles where the signals for mCLING and the two immunostained proteins colocalized. Bar, 2 µm. (B) Pearson's correlation coefficients were analyzed for the two markers immunostained in each experiment, selectively on mCLING-labeled organelles. Otoferlin and syntaxin 6 (or syntaxin 16) correlate in the mCLING-labeled organelles at the top and nuclear levels. VGLUT3 correlates best with otoferlin at the basal level. At least 100 organelles were analyzed for each condition. Error bars show SEMs. (C) Model of membrane recycling in IHCs. Organelles with different molecular composition recycle membrane in different regions, taking up mCLING. Apical endocytosis takes up membrane into round organelles, a sizeable proportion of which is similar to late endosomes (light blue). Endocytosis in the top and nuclear regions reaches tubular organelles containing otoferlin and two endosome markers, syntaxin 16 and syntaxin 6. This suggests that these organelles participate in constitutive pathways, probably by maintaining membrane traffic between the plasma membrane and the trans-Golgi. At the base of the cell, stimulation induces the formation of membrane infoldings and cisterns that are characterized by the presence of VGLUT3, Rab3, and also otoferlin.

Atwood et al., 1993 for a description of the morphology of this synapse). mCLING stained the large subsynaptic reticulum that surrounds the synaptic bouton as well as the bouton plasma membrane (Fig. S5, A and B). STED microscopy also allowed us to observe endocytotic intermediates forming upon stimulation, which were compatible with membrane infoldings already described in *Drosophila* synapses (for example, Koenig and Ikeda, 1996).

### mCLING applications to cultured neurons: Investigation of actively and spontaneously recycling synaptic vesicles

To test the usefulness of mCLING in smaller synapses, we turned to synaptic vesicle recycling in hippocampal neurons. Although this preparation has been studied intensively as a model for synaptic vesicle recycling, several fundamental issues are still open. For example, it is not yet clear whether the molecular composition of the vesicles that recycle upon stimulation (actively) is the same as that of vesicles that recycle spontaneously, in the absence of stimulation. Several works have suggested that active and spontaneous exocytosis use different vesicles (see for example Sara et al., 2005; Mathew et al., 2008; Fredj and Burrone, 2009; Chung et al., 2010), whereas others have claimed the contrary (Groemer and Klingauf, 2007; Hua et al., 2010; Wilhelm et al., 2010). More recently, spontaneously recycling vesicles have been suggested to preferentially contain molecular markers, such as the endosomal SNARE proteins VAMP7 (vesicle-associated membrane protein 7) or Vti1a (Hua et al., 2011; Ramirez et al., 2012).

To solve this question, we performed a broader analysis of the vesicle composition using mCLING as an endocytosis marker (after verifying that mCLING does not affect the properties of synaptic vesicle recycling in these neurons; Fig. S1 G). We stimulated synaptic boutons to cause the active recycling of synaptic vesicles (field stimulation at 20 Hz for 30 s). Alternatively, we incubated the cultured neurons in the presence of tetrodotoxin for 15 min to allow vesicles to recycle spontaneously (Wilhelm et al., 2010). The preparations were then immunostained for five synaptic vesicle proteins and three endosomal proteins (Fig. 8 A, experimental scheme), were sectioned at a thickness of 40–50 nm (about the size of one synaptic vesicle), and were analyzed by two-color STED microscopy.

mCLING-labeled vesicles were visible inside synaptic boutons (Fig. 8 B), containing various levels of immunostained proteins (Fig. 8 C). An analysis of the level of protein enrichment in the vesicles suggested several quantitative differences between spontaneously and actively recycling vesicles. The spontaneously recycling vesicles contained indeed higher levels of endosomal proteins (see also Hua et al., 2011; Ramirez et al., 2012). They also contained substantially lower levels of three synaptic vesicle proteins, synaptotagmin 1, VAMP2 (synaptobrevin 2), and synapsin, although they had similar levels of vesicular glutamate transporter or synaptophysin. This suggests that the presence of endosomal SNAREs is not the only difference between spontaneously and actively recycling vesicular membranes. The former may be more related to constitutively recycling membranes.

### mCLING applications to cultured neurons: Investigation of synaptic vesicle proteins on the plasma membrane

Just as the membrane of endocytotic organelles, the plasma membrane is difficult to observe in immunostaining experiments. In a typical immunostaining experiment, several proteins are identified, but the outline of the cell, the plasma membrane,

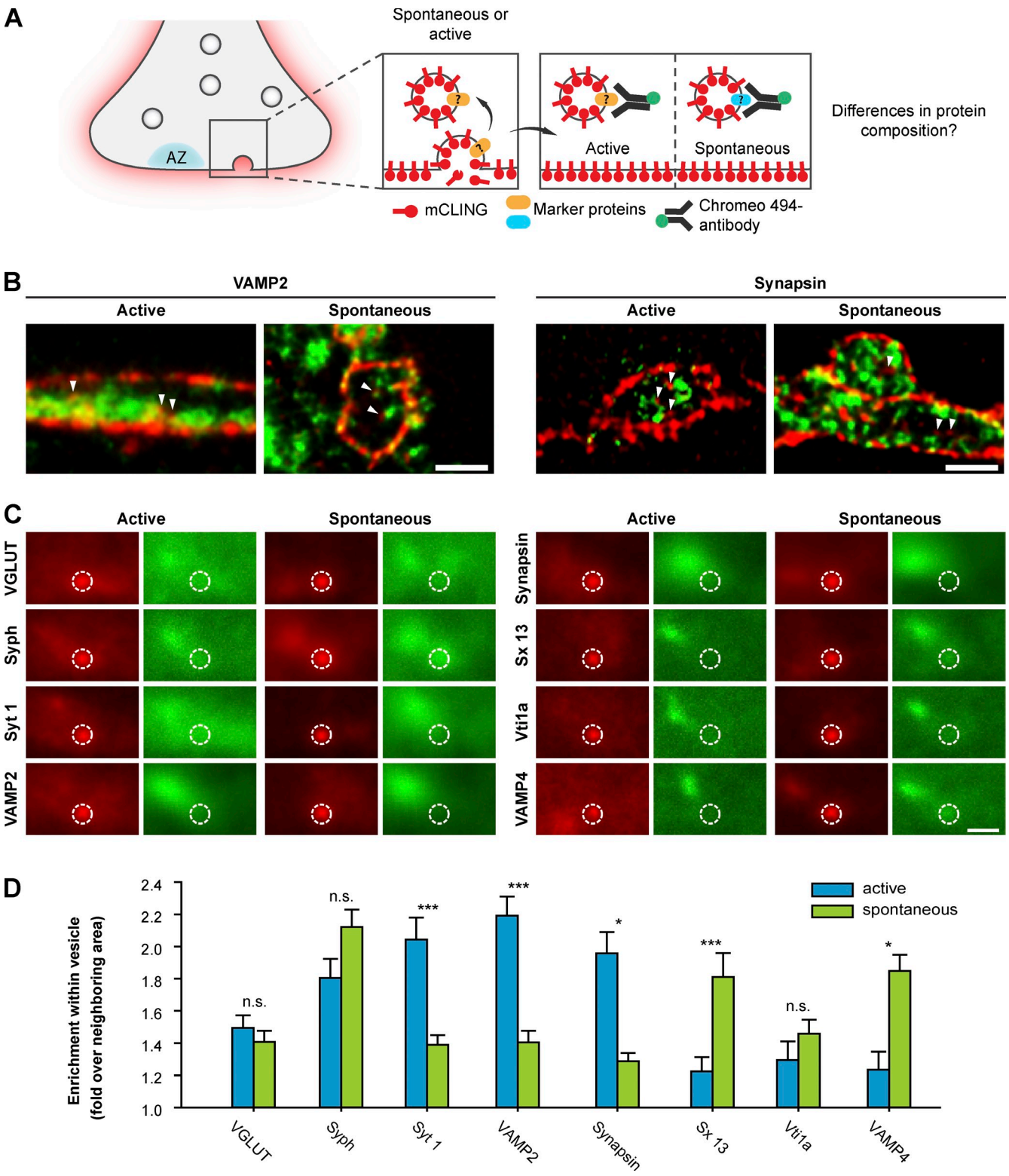


Figure 8. **mCLING reveals differences in protein composition between actively and spontaneously recycling synaptic vesicles in hippocampal neurons.** (A) Experimental outline: neurons are incubated with mCLING, and active synaptic vesicle recycling is induced by stimulation. Alternatively, spontaneous vesicle recycling is allowed to take place, whereas the neurons are silenced using tetrodotoxin. The preparations are then immunostained, embedded in melamine, cut in thin sections, and imaged using two-color STED microscopy, which allows the investigation of the vesicle composition. AZ, active zone. (B) Typical images of mCLING-labeled synaptic boutons. Proteins are shown in green, and mCLING is shown in red. Arrowheads point to several endocytosed vesicles. (C) Average images of mCLING-labeled vesicles from stimulated or resting preparations. Red images show the mCLING signal; green images show the corresponding immunostaining signals. The circles indicate the vesicle area; note that this contains abundant staining for some, but not all, of the proteins. The larger protein-stained area, shown at the left of the green images, represents the synaptic vesicle cluster. (D) The enrichment of the different proteins of interest within the vesicles was calculated, over the neighboring areas within the synapse. The error bars show means ± SEM from 100 to 500 mCLING-labeled vesicles. n.s., no significant difference (*t* test, $P > 0.05$); *, significant difference (*t* test, $P \leq 0.05$); ***, significant difference (*t* test, $P \leq 0.001$). Syph, synaptophysin; Sx 13, syntaxin 13; VGLUT, vesicular glutamate transporter; Syt 1, synaptotagmin 1. Bars, 500 nm.

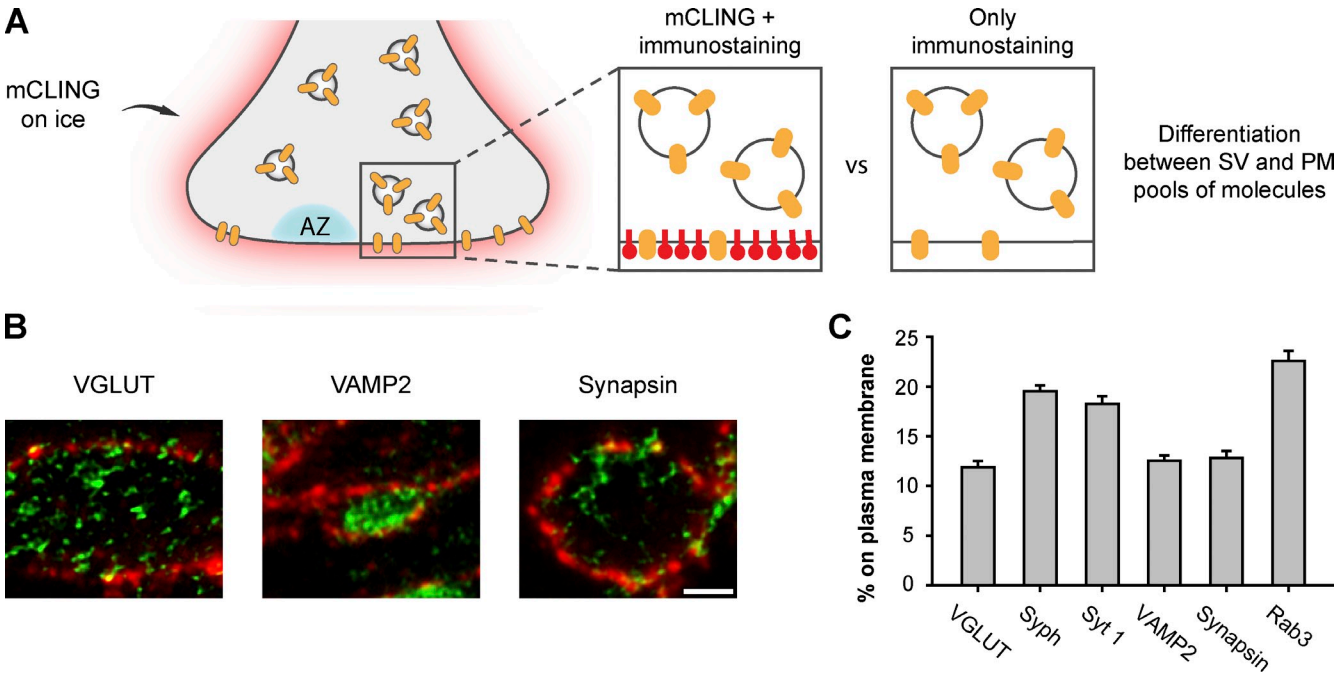


Figure 9. **mCLING use in identifying the membrane-associated fraction of synaptic vesicle proteins.** (A) Experimental outline: application of mCLING on ice reveals only the plasma membrane (PM). Immunostaining then allows the differentiation between membrane-associated staining and organelle-associated staining, which is further away from the membrane. (right) Without mCLING, the two cannot be differentiated. AZ, active zone; SV, synaptic vesicle. (B) Example two-color STED images. Proteins are shown in green, and mCLING is shown in red. Bar, 500 nm. (C) Analysis of the percentage of protein associated with the plasma membrane. The error bars show means ± SEM from 99 to 270 mCLING-labeled membrane areas. Syph, synaptophysin; Syt 1, synaptotagmin 1; VGLUT, vesicular glutamate transporter.

remains invisible. This is important, especially when investigating membrane-attached proteins. This is easily addressed by mCLING incubation on ice (Fig. 4 B). We used mCLING to reveal the plasma membrane (Fig. 9 A), and we imaged the different proteins in two-color STED experiments, from sections 40–50 nm in thickness (Fig. 9 B). We measured the amounts of protein signal overlapping with the plasma membrane mCLING label and compared them to the total protein amounts in the axons. To avoid confusing proteins on the plasma membrane with docked synaptic vesicles, we only analyzed the protein levels associated with the high-intensity core of the mCLING membrane labeling—which reveals only the plasma membrane in this experiment, as the mCLING incubation was performed for 5 min on ice. We found that between ∼12 and 22% of the proteins were present on the plasma membrane, suggesting that relatively high amounts of all synaptic proteins may participate in the readily retrievable pool (Fig. 9 C; see Wienisch and Klingauf [2006] for a discussion of the readily retrievable pool). Clearly, these experiments would benefit from investigations with an even higher spatial resolution, which would permit the unambiguous determination of the area occupied by the membrane—even at resolutions comparable with the membrane thickness (see for example Xu et al., 2012). However, in the present state, our results nevertheless suggest that mCLING can be used for such determinations, in an easier fashion than in immunoelectron microscopy, with the precision of the result being limited only by the microscope performance, rather than that of the label.

The ability to use mCLING to localize the plasma membrane in immunostaining experiments could also be exploited to analyze the membrane organization of different elements (Fig. 10 A), such as SNARE proteins (Jahn and Scheller, 2006). This procedure enabled us to study the organization of the SNAREs SNAP-25 (Fig. 10 B) and syntaxin 1 (Fig. 10 C). We compared their clusters from the plasma membrane with the clusters they form in axonal organelles. Syntaxin 1, which has been proposed to form elaborate arrangements on the plasma membrane (Sieber et al., 2007; Bar-On et al., 2012), formed much smaller clusters in organelles. In contrast, no such changes could be observed for SNAP-25 (Fig. 10, B and C).

## Discussion

Our study offers a novel fluorescent membrane probe, mCLING, which can be used to label the plasma membrane and also to faithfully track endocytotic organelles. mCLING can be used easily in conjunction with fixation and immunostaining, in both cell culture and in tissue, unlike most commercially available dyes that are used for membrane labeling. Moreover, mCLING is, to our knowledge, the only fluorescent probe that can be used to reveal the morphology and identity of small endocytotic organelles (Figs. 5 and 6).

The identification of the molecular identities of endocytotic organelles is the area in which mCLING will likely be most important. Endocytotic markers have been used in IHCs for decades (Siegel and Brownell, 1986; Griesinger et al., 2002, 2004, 2005). Alternatively, the IHCs and other sensory receptors have been immunostained (Roux et al., 2006; Seal et al., 2008; Pangršič et al., 2010; Duncker et al., 2013), even with resolutions beyond the diffraction limit (Wahl et al., 2013). However, neither visualization of endocytotic markers nor imaging of immunostained

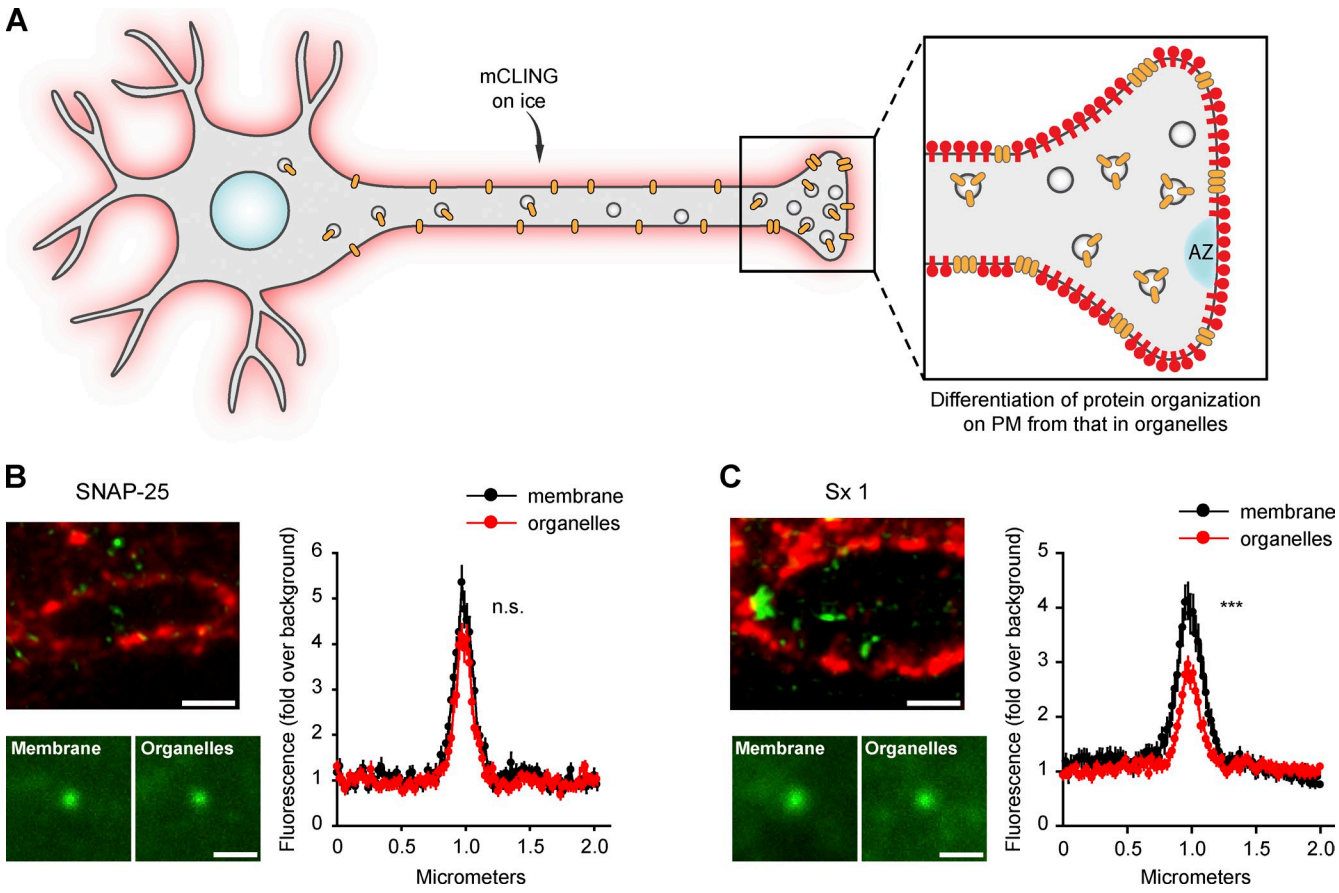


Figure 10. **mCLING use in revealing differences between organellar and plasma membrane protein assemblies.** (A) Experimental outline: as in Fig. 9, mCLING reveals the plasma membrane (PM) and allows the identification of protein clusters on the membrane or in intracellular organelles, away from the membrane. AZ, (B and C, top left) Example two-color STED images with mCLING in red and protein of interest in green (SNAP-25 or syntaxin 1 [Sx 1]). The bottom shows average images of the protein clusters, obtained by averaging 115–133 protein clusters from the membrane or from organelles for syntaxin 1 and 88–90 clusters for SNAP-25. (right) Average line scans through the protein clusters. Graphs show means ± SEM, from the same organelles. n.s., no significant difference in intensity between the peaks of the two distributions (*t* test, $P > 0.05$); ***, significant difference (*t* test, $P \leq 0.001$). Bars, 500 nm.

proteins has been sufficient to address the nature of the endocytotic organelles. This issue could only be solved by a method, such as mCLING imaging, in which both the endocytotic membranes and their protein markers were labeled at the same time (Figs. 6 and 7).

The ability of mCLING to reveal the plasma membrane at high resolution also provides an important advantage in imaging experiments. Numerous studies have reported the organization of neuronal proteins, either on axons or within the compact space of synapses (for example, Kittel et al., 2006; Willig et al., 2006; Dani et al., 2010; Denker et al., 2011; Wahl et al., 2013). In most of these cases, the ability to see the borders of the synaptic boutons would have added much information, especially in what concerns the spatial distributions of the protein clusters and the borders of the individual synaptic boutons. This will be an advantage both in synaptic systems, including cultured neurons, and in other cell types.

Finally, we would like to point out that mCLING imaging could also be extended to different processes and not only to the membrane trafficking (endocytotic) pathway. For example, the structure and molecular organization of isolated organelles in vitro, or the arrangement of proteins on the membranes of various types of cells, can be easily tackled with mCLING. Such efforts will be aided in the future by the fact that mCLING is one of the few available probes that can be coupled to various fluorophores and can thus be optimized for any available super-resolution technique.

## Materials and methods

### mCLING validation on cultured cells

COS7 cells were cultured according to standard protocols. Cells were incubated with the different membrane and/or endocytosis markers in Ringer's buffer for 5 min at 37°C or on ice, at the following concentrations: 0.2–0.4 µM mCLING, 5 µM FM 1-43 (Biotium), 5 µM AM 1-43 (Biotium), 5 µM FM 4-64FX (Life Technologies), 25 µg/ml Alexa Fluor 546–Transferrin (Life Technologies), 0.4 ng/ml tetramethylrhodamine-EGF (Life Technologies), or 15 µg/ml DiI-LDL (Life Technologies). Cells were imaged live (in Ringer's buffer), fixed (4% PFA + 0.2% glutaraldehyde; Mowiol embedding), or fixed and permeabilized (0.1% Triton X-100 + 2.5% BSA; Mowiol embedding), at RT in an inverted microscope (IX71; Olympus) equipped with a 60×, 1.35 NA oil immersion objective or a 100×, 1.45 NA TIRFM (total internal reflection fluorescence microscopy) oil immersion objective (Olympus) and a 100-W mercury lamp (Olympus). Images were acquired using the software cell^P (version 3.4; Olympus) and a charge-coupled device camera (1,376 × 1,032 pixels, pixel size of 6.45 × 6.45 µm; F-View II; Olympus). For the viability assay (Fig. S1, C–E), COS7 cells were incubated in different concentrations of mCLING for 5 min, washed, and incubated

in Ringer's buffer containing propidium iodide. The cells were then imaged in an inverted epifluorescence microscope (Eclipse Ti-E; Nikon) equipped with a lamp (HBO-100W), a camera (IXON X3897; Andor Technology), and a CFI S Plan Fluor ELWD (Extra Long Working Distance; air) 40×, 0.60 NA objective (Nikon) and operated with the software NIS-Elements AR (version 4.20; Nikon). For confocal imaging of COS7 cells (Figs. 1 D and 2, B and C), the same microscope as for STED microscopy was used (as described in the STED microscopy section of the Materials and methods).

### mCLING validation on yeast and bacteria

*S. cerevisiae* cells from the strain BY4742 were immobilized on poly-L-lysine (PLL)–coated coverslips and labeled with either 20 µM FM 4-64 or 0.4 µM mCLING in YNB (yeast nitrogen base) medium for 20 min. Cells were imaged live (in YNB medium with the dye), fixed, or fixed and immunostained (same protocol as for COS7 cells; Mowiol embedded). Imaging was performed in the same Olympus microscope described in the previous section, using the 100×, 1.45 NA TIRFM oil immersion objective combined with an optovar lens of 1.6× magnification (Olympus). For membrane staining of *E. coli* cells, these were immobilized on PLL-coated coverslips and labeled with either 5 µM FM 1-43 or 0.4 µM mCLING, in LB medium, for 5 min. After washing and direct mounting in Mowiol, cells were imaged in confocal or super-resolution mode using the STED microscope described in the STED microscopy section of the Materials and methods.

### Animals

Mice (*Mus musculus*) from the wild-type substrains C57BL/6N and C57BL/6J were obtained from the animal facility of the University Medical Center Göttingen or from Charles River. Other mouse strains used included CD1/C57BL/6J expressing VGLUT1-pHluorin (offspring of CD1 mice mated with C57BL/6J mice) and Otoferlin knockout mice (*Otof*$^{-/-}$ mice; see next section of Materials and methods). Male or female mice, at ages between postnatal days 14 and 18, were used for organ of Corti dissection. Mice were handled according to the specifications of the University of Göttingen and of the state of Lower Saxony (Landesamt für Verbraucherschutz, Braunschweig, Germany).

### Mouse mutagenesis

To generate *Otof*$^{-/-}$ mice (described in Reisinger et al., 2011), a targeting vector was generated to replace exons 14 and 15 of the otoferlin wild-type gene by homologous recombination. A sequence containing 2.7- and 5.3-kb-long linkers upstream and downstream of a floxP-flanked neomycin selection cassette was subcloned into the NdeI and NsiI restriction sites of the respective gene intron regions (backbone vector pL253). 129ola embryonic stem cell colonies were electroporated with the targeting vector and selected with G418 and ganciclovir. After evaluating successful recombination by Southern blot analysis, positive clones were injected into mouse blastocysts for generation of chimeric mice. The heterozygous offspring of those mice were bred with cre recombinase–expressing mice to excise the neomycin cassette. Deletion of the neomycin cassette was confirmed by PCR. Absence of otoferlin from IHCs was confirmed by immunostaining using two different antibodies (mouse monoclonal, ab53233 [Abcam]; rabbit polyclonal, 178 003 [Synaptic Systems]).

### mCLING labeling and immunostaining in IHCs

The apical turn of the organ of Corti was dissected and directly placed in an imaging chamber filled with HBSS without calcium (HBSS without $Ca^{2+}$) containing (mM): 5.36 KCl, 141.7 NaCl, 1 $MgCl_2$, 0.5 $MgSO_4$, 10 Hepes, 3.4 L-glutamine, and 6.9 D-glucose, pH 7.4. For labeling, the organ of Corti was incubated with 1.7 µM mCLING. Incubation times were always of 3 min, to ensure adequate probe penetration into the tissue. For stimulation, organs were first incubated for 2 min in HBSS without $Ca^{2+}$ + mCLING and then for 1 min in HBSS high $K^+$ + mCLING (KCl increased to 65.36 mM, NaCl reduced to 79.7 mM, and 2 mM $CaCl_2$). For recovery after stimulation, the probe was washed off, and the sample was incubated for 5 min in a constant flow of dye-free HBSS with $Ca^{2+}$ (NaCl reduced to 139.7 mM plus 2 mM $CaCl_2$, with 5.36 mM KCl). All solutions were carbogen charged and prewarmed at 37°C before the experiments. After labeling, samples were rapidly washed with HBSS without $Ca^{2+}$, fixed in 4% PFA + 0.2% glutaraldehyde for 30 min on ice followed by 30 min at RT, and quenched in 100 mM $NH_4Cl$ + 100 mM glycine for 30 min. Afterward, organs were permeabilized in 0.5% Triton X-100 + 1.5% BSA in PBS (3 × 10 min) and incubated for 1 h with one of the following primary antibodies (diluted in PBS + 0.5% Triton X-100 + 1.5% BSA): calnexin (rabbit polyclonal, ab22595; Abcam), GM130 (mouse monoclonal, 610822; BD), LAMP1 (rabbit polyclonal, ab24170; Abcam), otoferlin (mouse monoclonal, ab53233; Abcam), Rab3 (mouse monoclonal, 610379; BD), syntaxin 6 (mouse monoclonal, 610636; BD), syntaxin 16 (rabbit polyclonal; provided by R. Jahn, Max Planck Institute for Biophysical Chemistry, Göttingen, Germany; same as 110 162 obtained from Synaptic Systems), VGLUT3 (rabbit polyclonal, 135203; Synaptic Systems), and Vti1a (mouse monoclonal, 611220; BD). After primary antibody incubation, washes with 0.5% Triton X-100 + 1.5% BSA in PBS (3 × 10 min) were performed. Secondary antibodies were Chromeo494-coupled goat anti–rabbit IgG (15042; Active Motif) and Chromeo494-coupled goat anti–mouse IgG (15032; Active Motif). For identifying the synaptic ribbon, the following antibodies were used: primary antibodies against CtBP2 (also recognizing Ribeye A domain; mouse monoclonal, 612044; BD) or Ribeye B domain (rabbit polyclonal, 192003; Synaptic Systems) and, as secondary antibodies, Cy2-coupled goat anti–mouse IgG or goat anti–rabbit IgG (115-225-146 and 111-225-144; Dianova). Finally, organs were washed with high salt PBS (containing 500 mM NaCl; 3 × 10 min) and standard PBS (2 × 10 min).

### Cell surface quenching of mCLING in IHCs

After mCLING labeling for 2 min in HBSS without $Ca^{2+}$ and 1 min under stimulation conditions (65 mM KCl), the organ of Corti was placed in an imaging chamber containing mCLING-free HBSS with $Ca^{2+}$ and 0.75 mM BPB for 5 min. BPB quenched the mCLING on the cell surface, enabling the live imaging of endocytotic organelles. IHCs were stimulated for a second time by replacing the solution with HBSS with high $K^+$ and 0.75 mM BPB (65 mM KCl for 1 min). In the control group, the second stimulation was performed in the absence of $Ca^{2+}$ and in the presence of 0.75 mM BPB and 5 mM EGTA. Live imaging was performed at RT using an upright confocal microscope (SP2; Leica) equipped with a HCX Apochromat L UV-visible-infrared 63×, 0.9 NA water immersion objective (Leica) and operated with the Leica Confocal Software (version 2.61; Leica).

### VGLUT1-pHluorin experiments in IHCs

Complementary DNA of pHluorin-coupled VGLUT1 (a gift from R. Edwards, University of California, San Francisco, San Francisco, CA) was subcloned into an AAV-HBA-EWB vector using an EcoRI and a HindIII restriction site introduced through PCR. The virus was produced by S. Kügler (University Medical Center Göttingen, Göttingen, Germany) as described previously (Kügler et al., 2007), using capsid proteins of serotype 1 and 2 (AAV1/2). IHCs were transduced by trans-uterine injection of otocysts in postcoital day 11.5 pregnant CD1 dams mated with C57BL/6J males (Bedrosian et al., 2006). The live imaging of transduced IHCs was performed with a confocal microscope (FluoView 300) equipped with a 60×, 0.9 NA water-immersion objective, all obtained from Olympus (Frank et al., 2009). pHluorin and TAMRA (carboxytetramethylrhodamine)-conjugated Ribeye-binding peptide (Zenisek et al., 2004) were excited with a 50-mW, 488-nm laser (Cyan; Newport Spectraphysics) and with a 1.5-mW, 543-nm He-Ne laser, respectively. Patch–clamp experiments were performed with an EPC 9 amplifier and Patchmaster software (HEKA) using intracellular solution containing (mM) 131.5 Cs-glutamate, 13 tetraethylammonium-Cl, 20 CsOH-Hepes, 1 $MgCl_2$, 2 MgATP, 0.3 NaGTP, 0.5 EGTA, and 0.04 Ribeye-binding peptide, pH 7.2, and extracellular solution containing 104 NaCl, 35 tetraethylammonium-Cl, 2.8 KCl, 5 $CaCl_2$, 1 $MgCl_2$, 10 NaOH-Hepes, and 10 D-glucose, pH 7.3.

### Neuronal culture methods

Neuronal hippocampal cultures were obtained from dissociated hippocampi of newborn rats (modified from Banker and Cowan, 1977; Beaudoin et al., 2012). In brief, brains were extracted from the skulls of postnatal 2-d-old rat pups, and the hippocampi were isolated under a dissection microscope. Following washes with HBSS (Invitrogen) to remove tissue debris, the hippocampi were incubated for 1 h in enzyme solution (10 ml DMEM, 2 mg cysteine, 100 mM $CaCl_2$, 50 mM EDTA, and 25 U sterile papain bubbled with carbogen for 10 min and sterile filtered). Before mechanical dissociation, cells were washed thoroughly with HBSS and incubated for 15 min in inactivating solution (2 mg albumin and 2 mg trypsin inhibitor in 10 ml FCS containing DMEM medium). Before seeding, coverslips were treated with nitric acid, washed thoroughly with sterile water, and 1 mg/ml PLL coated overnight. Dissociated neurons were seeded in plating medium (MEM supplemented with 10% horse serum, 3.3 mM glucose, and 2 mM glutamine) and incubated for 1–4 h at 37°C in a 5% $CO_2$ humidified atmosphere to allow adhesion to the substrate. After adhesion, the medium was changed to Neurobasal-A medium containing 500 ml Neurobasal-A (Gibco), 10 ml B27 supplement (Gibco), and 5 ml GlutaMAX I stock. To avoid glial proliferation 5-fluoro-2′-deoxyuridine was added to the culture after 2 d in vitro. The neurons were kept in culture at 37°C and 5% $CO_2$ for 14 d before use. mCLING

labeling (0.68 µM) and immunostaining were performed as for the IHCs, using the incubation and stimulation conditions indicated in the main text for the different experiments (see Results sections titled mCLING applications to cultured neurons). Tyrode buffer was used, containing 124 mM NaCl, 5 mM KCl, 2 mM $CaCl_2$, 30 mM glucose, and 25 mM Hepes, pH adjusted to 7.3. Permeabilization was performed with 0.1% Triton X-100 and 2.5% BSA. The following antibodies were used: VGLUT1/2 (rabbit polyclonal, 135 503; Synaptic Systems), synaptophysin (rabbit polyclonal raised against synaptophysin purified from rat synaptic vesicles; see Jahn et al., 1985; provided by R. Jahn), synaptotagmin 1 (rabbit polyclonal, 105 102; Synaptic Systems), VAMP2 (mouse monoclonal, 104211; Synaptic Systems), synapsin (rabbit polyclonal, 106 002; Synaptic Systems), syntaxin 13 (mouse monoclonal, 110 131; Synaptic Systems), Vti1a (mouse monoclonal, 611220; BD), VAMP4 (rabbit polyclonal, 136002; Synaptic Systems), Rab3a (rabbit polyclonal, 107 003; Synaptic Systems), syntaxin 1 (mouse monoclonal, 110 011; Synaptic Systems), and SNAP-25 (rabbit polyclonal, 111 002; Synaptic Systems). Chromeo494-coupled goat secondary antibodies were used accordingly.

To study the effects of mCLING on synaptic vesicle recycling, neurons were transfected with the synaptopHluorin plasmid using calcium phosphate (ProFection; Promega). The synaptopHluorin insert (a gift from L. Lagnado, University of Sussex, Brighton, England, UK) was subcloned into a pEGFP-N1 plasmid (cytomegalovirus promoter; Takara Bio Inc.) by PCR through insertion of a KpnI restriction site in the forward primer (5′-AATGGTACCGCCGGTCGCCACC-3′) and a NotI restriction site in the reverse primer (5′-AATGCGGCCGCTTTAACCGGTTTTGTATAG-3′). Recombinant clones were confirmed by sequencing. After 8 d in vitro, transfected neurons were treated with 0.2 µM mCLING for 5 min. Cells were then stimulated using an A385 stimulus isolator and an A310 Accupulser stimulator (World Precision Instruments). 100-mA shocks were delivered initially in a short stimulus (3 s at 20 Hz) and 40 s later in a long stimulus (30 s at 20 Hz). Spontaneous network activity was blocked after mCLING incubation using 10 µM 6-cyano-7-nitroquinoxaline-2,3-dione and 1 µM AP5. Imaging was performed in the same Nikon setup described in the first Materials and methods section using a Plan Apochromat 60×, 1.4 NA oil immersion objective.

### *Drosophila* methods

Third instar larvae were dissected, internal organs were removed, and the larvae were pinned as previously described (Jan and Jan, 1976). The larvae were preincubated during 2 min with 1.7 µM mCLING and then electrically stimulated in *Drosophila* saline (Jan and Jan, 1976) at 20 Hz for 8 s before fixation (same as organs of Corti). Active zones were identified by immunostaining against Bruchpilot (mouse monoclonal, nc82; Developmental Studies Hybridoma Bank at The University of Iowa, Iowa City, IA).

### Embedding in polymer resin for fluorescence imaging

The resin hardener was prepared by dissolving 48 mg *p*-toluenesulfonic acid monohydrate (Sigma-Aldrich) in 0.576-ml distilled water. 1.344 g 2,4,6-Tris[bis(methoxymethyl)amino]-1,3,5-triazine (melamine) was added, and the tube was agitated on a horizontal shaker at 250 rpm for 2 h or until the melamine was completely dissolved. After mCLING labeling and immunostaining (see mCLING labeling and immunostaining in IHCs), the organ of Corti was placed (tectorial membrane facing down) on an 18-mm glass coverslip. A BEEM capsule (BEEM, Inc.), whose bottom had previously been cut, was placed with the opening down, surrounding the organ of Corti. 200 µl of freshly prepared melamine was poured inside the BEEM capsule, covering the organ of Corti completely. The mounted sample was placed in a box containing silica beads for removing the water and left overnight at RT to allow penetration of melamine into the tissue. The box was then heated to 40°C for 24 h. The BEEM capsule was filled to the top with Epon resin (EpoFix kit; Struers) and then heated up at 60°C for 48 h. The melamine around the organ of Corti was trimmed away with a scalpel blade, and samples were again incubated at 60°C for 48 h for complete hardening. Melamine blocks were cut into thin sections with an ultramicrotome (EM UC6; Leica). Sections were dried on a coverslip and embedded in Mowiol for two-color STED or epifluorescence imaging at RT.

### STED microscopy

A STED microscope (TCS SP5; Leica) equipped with a HCX Plan Aprochromat 100×, 1.4 NA oil STED objective and operated with the LAS AF imaging software (version 2.7.3.9723; Leica) was used for performing two-color STED microscopy. Chromeo494 and Atto647N were excited with pulsed diode lasers (PDL 800-D; PicoQuant) at 531 and 640 nm, respectively. The STED beam was generated by a Ti:Sapphire laser (Mai Tai; Spectra-Physics) tuned at 750 nm. The same microscope was used for acquiring confocal images of COS7 cells using an HCX Plan Apochromat 63×, 1.4 NA oil immersion objective.

### Thin-section imaging

mCLING-labeled organs of Corti were fixed and immunostained for VGLUT3 and otoferlin, VGLUT3 and syntaxin 6, otoferlin and syntaxin 16, or syntaxin 6 and syntaxin 16 as described previously in this paper. The same primary antibodies used for the double labeling (see the section mCLING labeling and immunostaining in IHCs from the Materials and methods) were recognized by Cy3- and Cy2-coupled goat anti–mouse IgG or goat anti–rabbit IgG (115-225-146 and 111-225-144) accordingly. After melamine embedding, 20-nm-thick sections were cut and imaged at RT using the same epifluorescence inverted microscope (IX71) described in the first Materials and methods section. Images were acquired with a 100×, 1.45 NA TIRFM oil immersion objective (Olympus).

### Data analysis

For presentation purposes, the STED images were deconvolved with the software Huygens Essential 4.4 (Scientific Volume Imaging), based on a CMLE (Classical Maximum Likelihood Estimation) algorithm. The in-built deconvolution functions of the software were adapted to the imaging parameters of the aforementioned STED microscope. Images were processed and arranged for display using Photoshop and Illustrator software (Adobe).

For calculating endocytosis levels (Fig. 4 D), we analyzed nondeconvolved STED images from transversal cuts of mCLING-labeled IHCs. Images were processed with a self-written MATLAB (The MathWorks, Inc.) routine to determine the percentage of the cellular region occupied by mCLING-labeled organelles. mCLING-labeled organelles were defined as groups of pixels with fluorescence intensities above the mean mCLING background value. A similar routine was used in Fig. 4 G, determining the mCLING intensity levels, rather than the area occupied. Similar routines were used in Fig. 9. The macros are found in zip file 1.

To establish the presence of various proteins on mCLING-labeled organelles (Figs. 6 and 7), we analyzed two-color STED or epifluorescence images taken from transversal cuts of mCLING-labeled and immunostained IHCs. A self-written MATLAB routine was used to calculate Pearson's correlation coefficients between line scans (20 pixels long and 2 pixels wide, using 20.2-nm pixels) drawn on organelles in both channels. The macros are found in zip file 2.

To obtain averaged STED pictures of IHC active zones (Fig. 5), we selected for each condition ≥20 regions of interest (ROIs; 5 × 5 $\mu m^2$) centered on synaptic ribbons. Using a self-written MATLAB routine, we rotated the ROIs until we obtained the maximum overlap, measured both in the mCLING and immunostaining channels. A final grayscale image of the average fluorescence intensities was then generated from the stack of individual images. The average images are displayed using the Jet lookup table inbuilt in ImageJ (National Institutes of Health). Similar routines were used to identify and average the neuronal organelles (Fig. 8) or SNARE clusters (Fig. 10). The macros are found in zip file 3.

### Statistical analysis

All graphs show means ± SEM, unless otherwise indicated in the figure legends. The *t* test (unpaired) was used (p-values indicated in the figure legends). No blinding was used for data analysis, as each dataset could be easily recognized by the experimenters.

### Online supplemental material

Fig. S1 shows the poor fixability of Atto647N-coupled PLL chains and that mCLING is not toxic, does not interfere with membrane trafficking processes in cultured cells, and does not affect synaptic vesicle recycling in hippocampal neurons. Fig. S2 shows the suitability of mCLING for imaging membranes of *E. coli* cells under STED microscopy. Fig. S3 shows that endocytosis in IHCs is clathrin and dynamin dependent and that synaptic vesicle exocytosis preferentially occurs at the active zones of IHCs, as indicated by pHluorin imaging. Fig. S4 shows that endocytosis at the cuticular level of IHCs is related to constitutive trafficking to late endosomes/lysosomes. Fig. S5 shows mCLING uptake at the *Drosophila* larval neuromuscular junction. Three ZIP files are provided containing self-written MATLAB routines: The routine zip file 1 was used to calculate the percentage of cellular area occupied by mCLING-labeled organelles. The routine zip file 2 was used to calculate Pearson's correlation values between the mCLING and the immunostaining channels across mCLING-labeled organelles. The routine zip file 3 was used to generate average pictures of aligned ribbon-type active zones and to generate average images of mCLING-labeled and

immunostained synaptic vesicles. Online supplemental material is available at http://www.jcb.org/cgi/content/full/jcb.201402066/DC1.

We thank Katharina Kröhnert and Christina Schäfer for expert technical assistance. We thank Jakob Neef and Eugenio F. Fornasiero for experimental advice and assistance. We thank Goran Kokic for experimental assistance with *Drosophila* preparations. We thank Sebastian Kügler (University Medical Center Göttingen) for providing the viral vector. We thank Profs. Reinhard Jahn (Max Plank Institute for Biophysical Chemistry, Göttingen, Germany), Robert Edwards (University of California, San Francisco, San Francisco, CA), and Leon Lagnado (University of Sussex, Brighton, England, UK) for providing reagents.

This work was supported by a grant from the Deutsche Forschungsgemeinschaft through the Collaborative Research Center 889 "Cellular Mechanisms of Sensory Processing'" (to S.O. Rizzoli, E. Reisinger, and T. Moser), by the Cluster of Excellence Nanoscale Microscopy and Molecular Physiology of the Brain (grant to S.O. Rizzoli and T. Moser), and by a Starting Grant from the European Research Council, Program FP7 (NANOMAP; to S.O. Rizzoli).

The authors declare no competing financial interests.

Submitted: 13 February 2014
Accepted: 14 April 2014

## References

Atwood, H.L., C.K. Govind, and C.F. Wu. 1993. Differential ultrastructure of synaptic terminals on ventral longitudinal abdominal muscles in *Drosophila* larvae. *J. Neurobiol.* 24:1008–1024. http://dx.doi.org/10.1002/neu.480240803

Banker, G.A., and W.M. Cowan. 1977. Rat hippocampal neurons in dispersed cell culture. *Brain Res.* 126:397–425. http://dx.doi.org/10.1016/0006-8993(77)90594-7

Bar-On, D., S. Wolter, S. van de Linde, M. Heilemann, G. Nudelman, E. Nachliel, M. Gutman, M. Sauer, and U. Ashery. 2012. Super-resolution imaging reveals the internal architecture of nano-sized syntaxin clusters. *J. Biol. Chem.* 287:27158–27167. http://dx.doi.org/10.1074/jbc.M112.353250

Beaudoin, G.M.J., III, S.-H. Lee, D. Singh, Y. Yuan, Y.-G. Ng, L.F. Reichardt, and J. Arikkath. 2012. Culturing pyramidal neurons from the early postnatal mouse hippocampus and cortex. *Nat. Protoc.* 7:1741–1754. http://dx.doi.org/10.1038/nprot.2012.099

Bedrosian, J.C., M.A. Gratton, J.V. Brigande, W. Tang, J. Landau, and J. Bennett. 2006. In vivo delivery of recombinant viruses to the fetal murine cochlea: transduction characteristics and long-term effects on auditory function. *Mol. Ther.* 14:328–335. http://dx.doi.org/10.1016/j.ymthe.2006.04.003

Betz, W.J., F. Mao, and G.S. Bewick. 1992. Activity-dependent fluorescent staining and destaining of living vertebrate motor nerve terminals. *J. Neurosci.* 12:363–375.

Bonifacino, J.S., and B.S. Glick. 2004. The mechanisms of vesicle budding and fusion. *Cell.* 116:153–166. http://dx.doi.org/10.1016/S0092-8674(03)01079-1

Brandhorst, D., D. Zwilling, S.O. Rizzoli, U. Lippert, T. Lang, and R. Jahn. 2006. Homotypic fusion of early endosomes: SNAREs do not determine fusion specificity. *Proc. Natl. Acad. Sci. USA.* 103:2701–2706. http://dx.doi.org/10.1073/pnas.0511138103

Chung, C., B. Barylko, J. Leitz, X. Liu, and E.T. Kavalali. 2010. Acute dynamin inhibition dissects synaptic vesicle recycling pathways that drive spontaneous and evoked neurotransmission. *J. Neurosci.* 30:1363–1376. http://dx.doi.org/10.1523/JNEUROSCI.3427-09.2010

Dani, A., B. Huang, J. Bergan, C. Dulac, and X. Zhuang. 2010. Superresolution imaging of chemical synapses in the brain. *Neuron.* 68:843–856. http://dx.doi.org/10.1016/j.neuron.2010.11.021

Denker, A., K. Kröhnert, J. Bückers, E. Neher, and S.O. Rizzoli. 2011. The reserve pool of synaptic vesicles acts as a buffer for proteins involved in synaptic vesicle recycling. *Proc. Natl. Acad. Sci. USA.* 108:17183–17188. http://dx.doi.org/10.1073/pnas.1112690108

Duncker, S.V., C. Franz, S. Kuhn, U. Schulte, D. Campanelli, N. Brandt, B. Hirt, B. Fakler, N. Blin, P. Ruth, et al. 2013. Otoferlin couples to clathrin-mediated endocytosis in mature cochlear inner hair cells. *J. Neurosci.* 33:9508–9519. http://dx.doi.org/10.1523/JNEUROSCI.5689-12.2013

Frank, T., D. Khimich, A. Neef, and T. Moser. 2009. Mechanisms contributing to synaptic $Ca^{2+}$ signals and their heterogeneity in hair cells. *Proc. Natl. Acad. Sci. USA.* 106:4483–4488. http://dx.doi.org/10.1073/pnas.0813213106

Frank, T., M.A. Rutherford, N. Strenzke, A. Neef, T. Pangršič, D. Khimich, A. Fejtova, E.D. Gundelfinger, M.C. Liberman, B. Harke, et al. 2010. Bassoon and the synaptic ribbon organize $Ca^{2+}$ channels and vesicles to add release sites and promote refilling. *Neuron.* 68:724–738. http://dx.doi.org/10.1016/j.neuron.2010.10.027

Fredj, N.B., and J. Burrone. 2009. A resting pool of vesicles is responsible for spontaneous vesicle fusion at the synapse. *Nat. Neurosci.* 12:751–758. http://dx.doi.org/10.1038/nn.2317

Gale, J.E., W. Marcotti, H.J. Kennedy, C.J. Kros, and G.P. Richardson. 2001. FM1-43 dye behaves as a permeant blocker of the hair-cell mechanotransducer channel. *J. Neurosci.* 21:7013–7025.

Glowatzki, E., and P.A. Fuchs. 2002. Transmitter release at the hair cell ribbon synapse. *Nat. Neurosci.* 5:147–154. http://dx.doi.org/10.1038/nn796

Goutman, J.D., and E. Glowatzki. 2007. Time course and calcium dependence of transmitter release at a single ribbon synapse. *Proc. Natl. Acad. Sci. USA.* 104:16341–16346. http://dx.doi.org/10.1073/pnas.0705756104

Griesinger, C.B., C.D. Richards, and J.F. Ashmore. 2002. Fm1-43 reveals membrane recycling in adult inner hair cells of the mammalian cochlea. *J. Neurosci.* 22:3939–3952.

Griesinger, C.B., C.D. Richards, and J.F. Ashmore. 2004. Apical endocytosis in outer hair cells of the mammalian cochlea. *Eur. J. Neurosci.* 20:41–50. http://dx.doi.org/10.1111/j.0953-816X.2004.03452.x

Griesinger, C.B., C.D. Richards, and J.F. Ashmore. 2005. Fast vesicle replenishment allows indefatigable signalling at the first auditory synapse. *Nature.* 435:212–215. http://dx.doi.org/10.1038/nature03567

Groemer, T.W., and J. Klingauf. 2007. Synaptic vesicles recycling spontaneously and during activity belong to the same vesicle pool. *Nat. Neurosci.* 10:145–147. http://dx.doi.org/10.1038/nn1831

Harata, N.C., A.M. Aravanis, and R.W. Tsien. 2006. Kiss-and-run and full-collapse fusion as modes of exo-endocytosis in neurosecretion. *J. Neurochem.* 97:1546–1570. http://dx.doi.org/10.1111/j.1471-4159.2006.03987.x

Hell, S.W. 2007. Far-field optical nanoscopy. *Science.* 316:1153–1158. http://dx.doi.org/10.1126/science.1137395

Hoopmann, P., A. Punge, S.V. Barysch, V. Westphal, J. Bückers, F. Opazo, I. Bethani, M.A. Lauterbach, S.W. Hell, and S.O. Rizzoli. 2010. Endosomal sorting of readily releasable synaptic vesicles. *Proc. Natl. Acad. Sci. USA.* 107:19055–19060. http://dx.doi.org/10.1073/pnas.1007037107

Hua, Y., R. Sinha, M. Martineau, M. Kahms, and J. Klingauf. 2010. A common origin of synaptic vesicles undergoing evoked and spontaneous fusion. *Nat. Neurosci.* 13:1451–1453. http://dx.doi.org/10.1038/nn.2695

Hua, Z., S. Leal-Ortiz, S.M. Foss, C.L. Waites, C.C. Garner, S.M. Voglmaier, and R.H. Edwards. 2011. v-SNARE composition distinguishes synaptic vesicle pools. *Neuron.* 71:474–487. http://dx.doi.org/10.1016/j.neuron.2011.06.010

Jahn, R., and R.H. Scheller. 2006. SNAREs—engines for membrane fusion. *Nat. Rev. Mol. Cell Biol.* 7:631–643. http://dx.doi.org/10.1038/nrm2002

Jahn, R., W. Schiebler, C. Ouimet, and P. Greengard. 1985. A 38,000-dalton membrane protein (p38) present in synaptic vesicles. *Proc. Natl. Acad. Sci. USA.* 82:4137–4141. http://dx.doi.org/10.1073/pnas.82.12.4137

Jan, L.Y., and Y.N. Jan. 1976. Properties of the larval neuromuscular junction in *Drosophila melanogaster*. *J. Physiol.* 262:189–214.

Kachar, B., A. Battaglia, and J. Fex. 1997. Compartmentalized vesicular traffic around the hair cell cuticular plate. *Hear. Res.* 107:102–112. http://dx.doi.org/10.1016/S0378-5955(97)00027-0

Kamin, D., N.H. Revelo, and S.O. Rizzoli. 2014. FM dye photo-oxidation as a tool for monitoring membrane recycling in inner hair cells. *PLoS ONE.* 9:e88353. http://dx.doi.org/10.1371/journal.pone.0088353

Khimich, D., R. Nouvian, R. Pujol, S. Tom Dieck, A. Egner, E.D. Gundelfinger, and T. Moser. 2005. Hair cell synaptic ribbons are essential for synchronous auditory signalling. *Nature.* 434:889–894. http://dx.doi.org/10.1038/nature03418

Kittel, R.J., C. Wichmann, T.M. Rasse, W. Fouquet, M. Schmidt, A. Schmid, D.A. Wagh, C. Pawlu, R.R. Kellner, K.I. Willig, et al. 2006. Bruchpilot promotes active zone assembly, Ca2+ channel clustering, and vesicle release. *Science.* 312:1051–1054. http://dx.doi.org/10.1126/science.1126308

Koenig, J.H., and K. Ikeda. 1996. Synaptic vesicles have two distinct recycling pathways. *J. Cell Biol.* 135:797–808. http://dx.doi.org/10.1083/jcb.135.3.797

Kügler, S., R. Hahnewald, M. Garrido, and J. Reiss. 2007. Long-term rescue of a lethal inherited disease by adeno-associated virus-mediated gene transfer in a mouse model of molybdenum-cofactor deficiency. *Am. J. Hum. Genet.* 80:291–297. http://dx.doi.org/10.1086/511281

Lenzi, D., J. Crum, M.H. Ellisman, and W.M. Roberts. 2002. Depolarization redistributes synaptic membrane and creates a gradient of vesicles on the synaptic body at a ribbon synapse. *Neuron.* 36:649–659. http://dx.doi.org/10.1016/S0896-6273(02)01025-5

Mallard, F., B.L. Tang, T. Galli, D. Tenza, A. Saint-Pol, X. Yue, C. Antony, W. Hong, B. Goud, and L. Johannes. 2002. Early/recycling endosomes-to-TGN transport involves two SNARE complexes and a Rab6 isoform. *J. Cell Biol.* 156:653–664. http://dx.doi.org/10.1083/jcb.200110081

Mathew, S.S., L. Pozzo-Miller, and J.J. Hablitz. 2008. Kainate modulates presynaptic GABA release from two vesicle pools. *J. Neurosci.* 28:725–731. http://dx.doi.org/10.1523/JNEUROSCI.3625-07.2008

Matthews, G., and P. Fuchs. 2010. The diverse roles of ribbon synapses in sensory neurotransmission. *Nat. Rev. Neurosci.* 11:812–822. http://dx.doi.org/10.1038/nrn2924

Meyers, J.R., R.B. MacDonald, A. Duggan, D. Lenzi, D.G. Standaert, J.T. Corwin, and D.P. Corey. 2003. Lighting up the senses: FM1-43 loading of sensory cells through nonselective ion channels. *J. Neurosci.* 23:4054–4065.

Miesenböck, G., D.A. De Angelis, and J.E. Rothman. 1998. Visualizing secretion and synaptic transmission with pH-sensitive green fluorescent proteins. *Nature*. 394:192–195. http://dx.doi.org/10.1038/28190

Neef, J., S. Jung, A.B. Wong, K. Reuter, T. Pangrsic, R. Chakrabarti, S. Kügler, C. Lenz, R. Nouvian, R.M. Boumil, et al. 2014. Modes and regulation of endocytic membrane retrieval in mouse auditory hair cells. *J. Neurosci.* 34:705–716. http://dx.doi.org/10.1523/JNEUROSCI.3313-13.2014

Nizak, C., S. Martin-Lluesma, S. Moutel, A. Roux, T.E. Kreis, B. Goud, and F. Perez. 2003. Recombinant antibodies against subcellular fractions used to track endogenous Golgi protein dynamics in vivo. *Traffic*. 4:739–753. http://dx.doi.org/10.1034/j.1600-0854.2003.00132.x

Pangršič, T., L. Lasarow, K. Reuter, H. Takago, M. Schwander, D. Riedel, T. Frank, L.M. Tarantino, J.S. Bailey, N. Strenzke, et al. 2010. Hearing requires otoferlin-dependent efficient replenishment of synaptic vesicles in hair cells. *Nat. Neurosci.* 13:869–876. http://dx.doi.org/10.1038/nn.2578

Pangršič, T., E. Reisinger, and T. Moser. 2012. Otoferlin: a multi-C2 domain protein essential for hearing. *Trends Neurosci.* 35:671–680. http://dx.doi.org/10.1016/j.tins.2012.08.002

Ramirez, D.M.O., M. Khvotchev, B. Trauterman, and E.T. Kavalali. 2012. Vti1a identifies a vesicle pool that preferentially recycles at rest and maintains spontaneous neurotransmission. *Neuron*. 73:121–134. http://dx.doi.org/10.1016/j.neuron.2011.10.034

Reisinger, E., C. Bresee, J. Neef, R. Nair, K. Reuter, A. Bulankina, R. Nouvian, M. Koch, J. Bückers, L. Kastrup, et al. 2011. Probing the functional equivalence of otoferlin and synaptotagmin 1 in exocytosis. *J. Neurosci.* 31:4886–4895. http://dx.doi.org/10.1523/JNEUROSCI.5122-10.2011

Roux, I., S. Safieddine, R. Nouvian, M. Grati, M.-C. Simmler, A. Bahloul, I. Perfettini, M. Le Gall, P. Rostaing, G. Hamard, et al. 2006. Otoferlin, defective in a human deafness form, is essential for exocytosis at the auditory ribbon synapse. *Cell*. 127:277–289. http://dx.doi.org/10.1016/j.cell.2006.08.040

Ruel, J., S. Emery, R. Nouvian, T. Bersot, B. Amilhon, J.M. Van Rybroek, G. Rebillard, M. Lenoir, M. Eybalin, B. Delprat, et al. 2008. Impairment of SLC17A8 encoding vesicular glutamate transporter-3, VGLUT3, underlies nonsyndromic deafness DFNA25 and inner hair cell dysfunction in null mice. *Am. J. Hum. Genet.* 83:278–292. http://dx.doi.org/10.1016/j.ajhg.2008.07.008

Sara, Y., T. Virmani, F. Deák, X. Liu, and E.T. Kavalali. 2005. An isolated pool of vesicles recycles at rest and drives spontaneous neurotransmission. *Neuron*. 45:563–573. http://dx.doi.org/10.1016/j.neuron.2004.12.056

Schmitz, F., A. Königstorfer, and T.C. Südhof. 2000. RIBEYE, a component of synaptic ribbons: a protein's journey through evolution provides insight into synaptic ribbon function. *Neuron*. 28:857–872. http://dx.doi.org/10.1016/S0896-6273(00)00159-8

Seal, R.P., O. Akil, E. Yi, C.M. Weber, L. Grant, J. Yoo, A. Clause, K. Kandler, J.L. Noebels, E. Glowatzki, et al. 2008. Sensorineural deafness and seizures in mice lacking vesicular glutamate transporter 3. *Neuron*. 57:263–275. http://dx.doi.org/10.1016/j.neuron.2007.11.032

Sieber, J.J., K.I. Willig, C. Kutzner, C. Gerding-Reimers, B. Harke, G. Donnert, B. Rammner, C. Eggeling, S.W. Hell, H. Grubmüller, and T. Lang. 2007. Anatomy and dynamics of a supramolecular membrane protein cluster. *Science*. 317:1072–1076. http://dx.doi.org/10.1126/science.1141727

Siegel, J.H., and W.E. Brownell. 1986. Synaptic and Golgi membrane recycling in cochlear hair cells. *J. Neurocytol.* 15:311–328. http://dx.doi.org/10.1007/BF01611434

Spicer, S.S., G.N. Thomopoulos, and B.A. Schulte. 1999. Novel membranous structures in apical and basal compartments of inner hair cells. *J. Comp. Neurol.* 409:424–437. http://dx.doi.org/10.1002/(SICI)1096-9861(19990705)409:3<424::AID-CNE7>3.0.CO;2-L

Spicer, S.S., C. Qu, N. Smythe, and B.A. Schulte. 2007. Mitochondria-activated cisternae generate the cell specific vesicles in auditory hair cells. *Hear. Res.* 233:40–45. http://dx.doi.org/10.1016/j.heares.2007.07.005

Vida, T.A., and S.D. Emr. 1995. A new vital stain for visualizing vacuolar membrane dynamics and endocytosis in yeast. *J. Cell Biol.* 128:779–792. http://dx.doi.org/10.1083/jcb.128.5.779

Wahl, S., R. Katiyar, and F. Schmitz. 2013. A local, periactive zone endocytic machinery at photoreceptor synapses in close vicinity to synaptic ribbons. *J. Neurosci.* 33:10278–10300. http://dx.doi.org/10.1523/JNEUROSCI.5048-12.2013

Wienisch, M., and J. Klingauf. 2006. Vesicular proteins exocytosed and subsequently retrieved by compensatory endocytosis are nonidentical. *Nat. Neurosci.* 9:1019–1027. http://dx.doi.org/10.1038/nn1739

Wilhelm, B.G., T.W. Groemer, and S.O. Rizzoli. 2010. The same synaptic vesicles drive active and spontaneous release. *Nat. Neurosci.* 13:1454–1456. http://dx.doi.org/10.1038/nn.2690

Willig, K.I., S.O. Rizzoli, V. Westphal, R. Jahn, and S.W. Hell. 2006. STED microscopy reveals that synaptotagmin remains clustered after synaptic vesicle exocytosis. *Nature*. 440:935–939. http://dx.doi.org/10.1038/nature04592

Xu, K., H.P. Babcock, and X. Zhuang. 2012. Dual-objective STORM reveals three-dimensional filament organization in the actin cytoskeleton. *Nat. Methods*. 9:185–188. http://dx.doi.org/10.1038/nmeth.1841

Zenisek, D., N.K. Horst, C. Merrifield, P. Sterling, and G. Matthews. 2004. Visualizing synaptic ribbons in the living cell. *J. Neurosci*. 24:9752–9759. http://dx.doi.org/10.1523/JNEUROSCI.2886-04.2004